iScience

CellPress
OPEN ACCESS

Article

HIV-Captured DCs Regulate T Cell Migration and Cell-Cell Contact Dynamics to Enhance Viral Spread

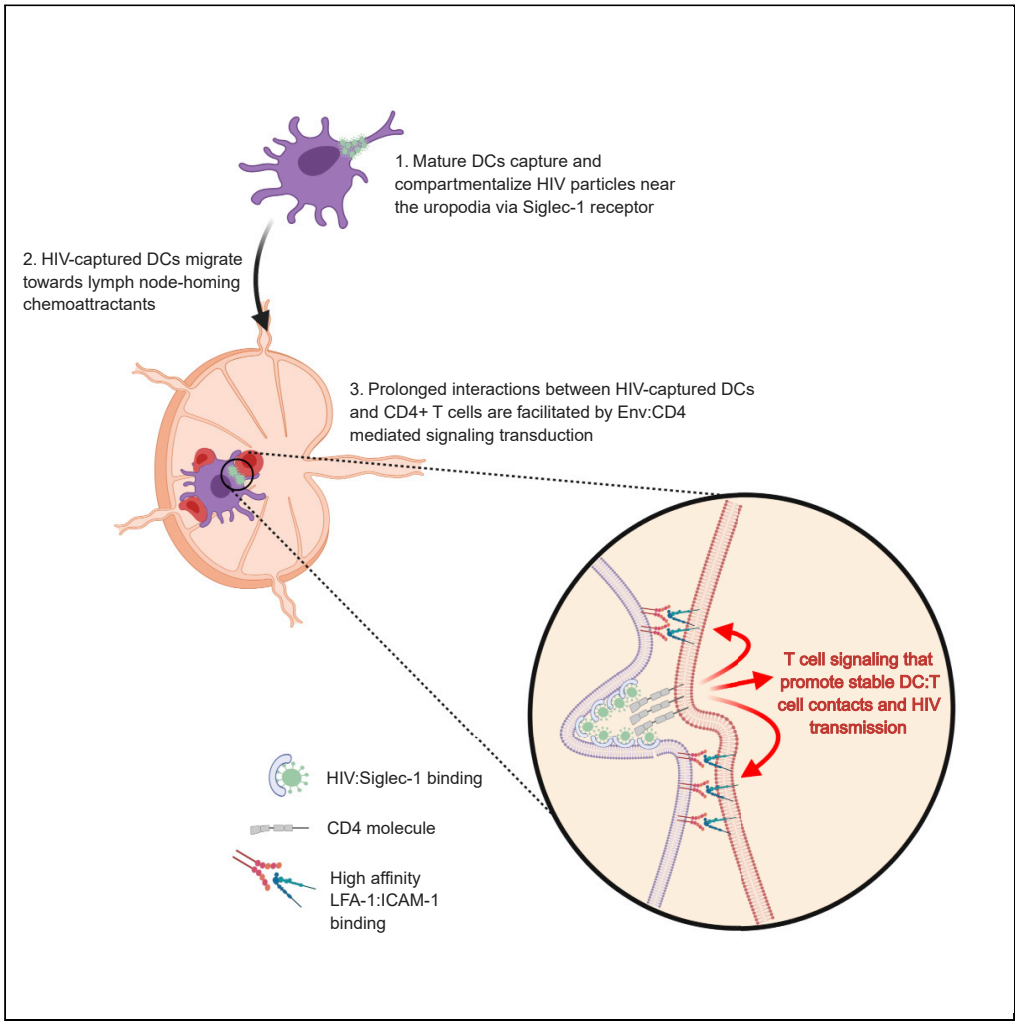

Wan Hon Koh, Paul Lopez, Oluwaseun Ajibola, ..., Ryan Hnatiuk, Jason Kindrachuk, Thomas T. Murooka

thomas.murooka@umanitoba.ca

HIGHLIGHTS

Mature DCs compartmentalize HIV particles near the uropodia via Siglec-1 receptor

HIV-captured DCs respond to lymph node-homing chemokines and access lymphatics

Prolonged contacts between HIV-captured DCs and CD4 T cells facilitate virus transfer

Surface-accessible HIV particles can induce T cell signaling via Env:CD4 engagement

Koh et al., iScience *23*, 101427
August 21, 2020 © 2020 The Author(s).
https://doi.org/10.1016/j.isci.2020.101427

iScience

CellPress
OPEN ACCESS

Article

HIV-Captured DCs Regulate T Cell Migration and Cell-Cell Contact Dynamics to Enhance Viral Spread

Wan Hon Koh,[1] Paul Lopez,[1] Oluwaseun Ajibola,[1] Roshan Parvarchian,[1] Umar Mohammad,[1] Ryan Hnatiuk,[1] Jason Kindrachuk,[2] and Thomas T. Murooka[1,2,3,*]

SUMMARY

Trafficking of cell-associated HIV-1 from the genital mucosa to lymphoid organs represents a critical first step toward systemic infection. Mature DCs capture and transmit HIV-1 to T cells, but insights into DC-to-T cell viral spread dynamics within a 3-dimensional environment is lacking. Using live-cell imaging, we show that mature DCs rapidly compartmentalize HIV-1 within surface-accessible invaginations near the uropod. HIV-1 capture did not interfere with DC migration toward lymph node homing chemo-attractants and their ability to enter lymphatic vessels. However, HIV-captured DCs engaged in prolonged contacts with autologous CD4+ T cells, which led to high T cell infection. Interestingly, we show that surface bound, virion-associated Env induced signal transduction in motile T cells that facilitated prolonged DC:T cell interactions, partially through high-affinity LFA-1 expression. Together, we describe a mechanism by which surface bound HIV-1 particles function as signaling receptors that regulate T cell motility, cell-cell contact dynamics, and productive infection.

INTRODUCTION

The majority of new human immunodeficiency virus-1 (HIV-1, referred to as HIV hereafter) infections worldwide occur through sexual mucosal transmission, of which young women are most vulnerable (Hladik et al., 2007; Piot et al., 2015; World Health Organization, 2018). During sexual transmission, HIV gains entry at mucosal sites (vaginal, penile, and anal mucosae) through breaks in the mucosal epithelial barrier to infect a founder population of susceptible targets (Baggaley et al., 2010; Haase, 2010, 2011; Tebit et al., 2012). During the eclipse phase of infection, focal clusters of infected cells replicate sufficient virus in mucosal T cells and macrophages that then leads to viral spread to draining and distant lymphoid organs (Haase, 2010, 2011; Rodriguez-Garcia et al., 2017). Our current understanding of viral dissemination kinetics following vaginal HIV infection come from studies with SIV-infected macaques (Miller et al., 2005), where locally infected cells in cervical vaginal tissues (CVTs) is followed by rapid dissemination into the draining lymph nodes (LNs), before spreading to distant lymphoid tissues and detection in blood (Deruaz et al., 2017; Haase, 2011; Hu et al., 2000; Masurier et al., 1998). Similar viral dissemination kinetics were also observed after vaginal challenge of BLT humanized mice (Deruaz et al., 2017) supporting the paradigm that HIV spread from the CVT to distant tissues is a stepwise progression of events that, once systemic dissemination is achieved, becomes difficult to eradicate with current drug regimens owing to the establishment of the latent reservoir (Whitney et al., 2014, 2018).

HIV reaches the genital-draining LN by two plausible mechanisms: (1) passive transport of infectious HIV particles released by infected CVT cells that enter the LNs via the lymphatics and (2) transport by infected or virus-carrying leukocytes via their natural trafficking into and within LNs, followed by their delivery to susceptible CD4+ T cells through cell-cell contact (Cunningham et al., 2010; Hladik et al., 2007; Jolly et al., 2004; Sigal et al., 2011). Although these mechanisms are not mutually exclusive, we previously showed that blocking leukocyte trafficking in and out of tissues after vaginal or subcutaneous HIV challenge in BLT humanized mice led to significant inhibition or delay in viremia and tissue viral loads (Deruaz et al., 2017; Murooka et al., 2012). Interfering with leukocyte recirculation in chronically infected animals did not impact viremia (Murooka et al., 2012), suggesting that HIV is actively carried into peripheral tissues and blood by migratory cells predominantly during the early stages of infection. More recently, we showed

[1]University of Manitoba, Rady Faculty of Health Sciences, Department of Immunology, Winnipeg, MB, Canada

[2]University of Manitoba, Rady Faculty of Health Sciences, Department of Medical Microbiology and Infectious Diseases, Winnipeg, Canada

[3]Lead Contact

*Correspondence: thomas.murooka@umanitoba.ca

https://doi.org/10.1016/j.isci.2020.101427

This is an open access article under the CC BY-NC-ND license (http://creativecommons.org/licenses/by-nc-nd/4.0/).

that enhanced migratory capacity of infected T cells, by disrupting Nef-mediated dysregulation of the actin cytoskeleton, accelerated systemic viral dissemination shortly after vaginal transmission, further implicating HIV-infected lymphocytes as motile vehicles for efficient viral spread (Usmani et al., 2019). Thus, HIV can hijack physiological immune surveillance, cellular trafficking and intercellular communication in order to evade immune recognition and reach large numbers of susceptible T cells in lymphoid organs (Fackler et al., 2014; Murooka and Mempel, 2013).

Cervical dendritic cells (DCs) can promote systemic viral spread through capture of infectious HIV particles and their transport to the draining lymph nodes, where virus is spread to susceptible T cells via cell-cell contact, termed DC *trans*-infection (Cameron et al., 1992; Geijtenbeek et al., 2000; Hu et al., 2004; Trifonova et al., 2018; Wu and KewalRamani, 2006). Although the cellular aspects of cell-cell HIV transmission are well described, most studies were done exclusively using culture systems that do not consider the highly motile nature and cell-cell contact dynamics between DCs and T cells observed in the lymph node. Another outstanding question is how DCs, in the absence of productive infection, restrain motile T cells to promote stable DC:T cell conjugates to facilitate viral transfer. We and others have utilized 3D collagen model systems to better characterize the dynamic on-off kinetics between infected and uninfected cells and have described key aspects of cell-cell contact behaviors that impact viral dissemination kinetics and pathogenesis (Lopez et al., 2019; Symeonides et al., 2015; Usmani et al., 2019). Herein, we addressed whether HIV-captured DCs retain their ability to exit the genital mucosae, enter the lymphatic vessels, and migrate toward LN-homing chemo-attractants and whether they can restrain motile T cells for long enough to permit viral transfer in the absence of cognate antigen recognition. We show that mature monocyte-derived DCs were highly efficient at capturing cell-free HIV particles which, over time, became condensed within compartments close to the uropodia of motile DCs. Consistent with previous studies, HIV particle capture was dependent on Siglec-1 and required actin cytoskeletal mobilization to compartmentalize virus for at least 24 h. HIV-captured DCs retain their ability to respond to tissue exit chemo-attractants CCL19/21 and S_1P by facilitating entry into and within lymphatic vessels. Using our 3D collagen imaging model, we show that CD4 T cells engaged in prolonged contacts with HIV-captured DCs that were dependent on gp120:CD4 interactions and further strengthened through LFA-1:ICAM-1 binding. Stable DC:T cell contacts resulted in increased T cell infection, highlighting an unexpected mechanism by which surface-bound HIV particles on DCs can function as adhesive receptors to contact and restrain motile T cells to facilitate HIV spread.

RESULTS

Mature Dendritic Cells Readily Capture and Compartmentalize HIV into Clusters near the Uropodia

Mature DCs capture and transmit infectious HIV particles to susceptible T cells more efficiently than immature DCs, whereas the latter are more susceptible to HIV infection (Turville et al., 2004). LPS-stimulated DCs upregulated HLA-DR, CD80/86, and CD83 and were more migratory compared with immature DCs in 3D collagen matrices (Figure S2). To better characterize HIV capture dynamics by motile DCs, we generated a dual-fluorescent HIV reporter that incorporates both the Gag-iGFP gene and *nef*-IRES-dTomato cassette (Gag-iGFP/dTomato).The resulting viral particles are brightly labeled by incorporation of the Gag-iGFP fusion protein, whereas infected cells express high levels of dTomato, allowing us to discriminate between productively infected ($GFP^+dTomato^+$) and HIV-captured but uninfected ($GFP^+dTomato^{neg}$) DCs and T cells (Figures 1A and S1). Cell surface CD4 downregulation was observed only in $dTomato^+$ cells, confirming functional Nef expression (Figure S1). Immature and LPS-stimulated MDDCs were incubated with virus for up to 28 h, and viral capture kinetics was evaluated by flow cytometry. As expected, mature DCs efficiently captured and retained HIV particles for up to 28 h, whereas immature DCs rapidly degraded HIV particles shortly after capture and only 2.6% of cells contained measurable HIV-iGFP after 28 h (Figures 1B and 1C). We did not observe infected, $dTomato^+$ only DCs during this time course experiment (Figure 1B). Next, we sought to visualize viral capture dynamics by DCs within a 3D fibrillar space that allowed cells to migrate and retain morphological features observed at mucosal surfaces *in vivo*. Celltracker blue-labeled DCs were co-embedded with HIV-iGFP particles in a 3D collagen matrix and visualized for up to 24 h (Figure 1D and Video S1). Although immature DCs remained immotile and weakly retained HIV clusters, mature DCs exhibited large dendritic extension, were migratory, and contained HIV particles. In the first hour, HIV particles were found dispersed throughout the cell, but over time, large viral clusters became visible near the trailing edge of migratory DCs, followed by distinct HIV compartmentalization by 5 h post-viral exposure (Figures 1D and 1E). This was confirmed by line profile analysis, showing that all DCs analyzed have compartmentalized virus by 24 h (Figure 1E). These studies confirm that mature DCs capture

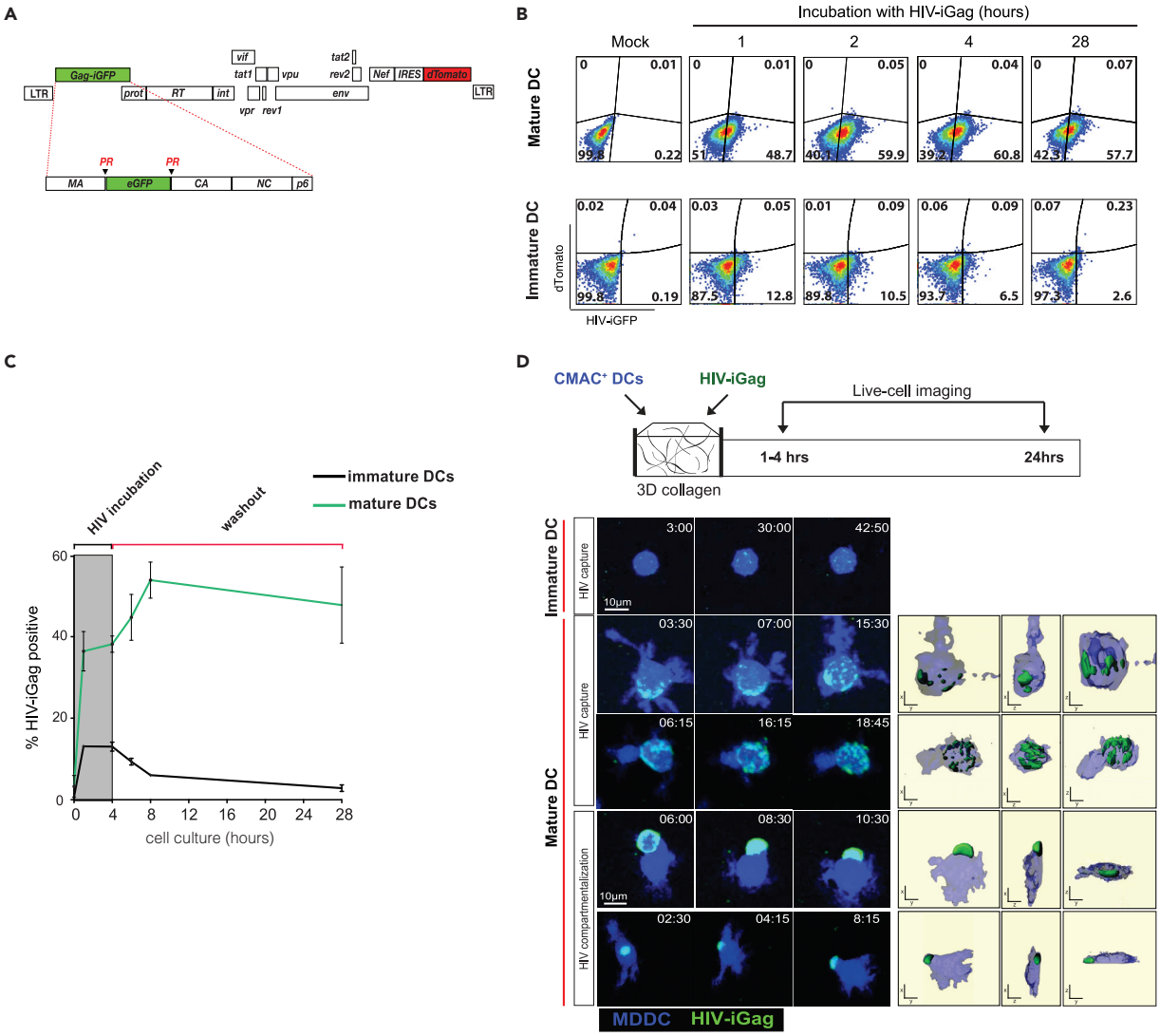
A
Gag-iGFP
vif
tat1
vpu
tat2
rev2
Nef
IRES
dTomato
LTR
prot
RT
int
env
vpr
rev1
PR
PR
MA
eGFP
CA
NC
p6
B
Incubation with HIV-iGag (hours)
Mock
1
2
4
28
Mature DC
Immature DC
dTomato
HIV-iGFP
C
HIV incubation
washout
immature DCs
mature DCs
% HIV-iGag positive
cell culture (hours)
D
CMAC+ DCs
HIV-iGag
Live-cell imaging
1-4 hrs
24hrs
3D collagen
Immature DC
Mature DC
HIV capture
HIV compartmentalization
MDDC
HIV-iGag
E
Line profile analysis
Trailing edge
Leading edge
HIV capture
HIV compartmentalization
HIV-iGag fluorescence (grey value)
Relative percentage
1 - 4 hrs
24hrs

Figure 1. HIV Capture Kinetics and Localization by Mature DCs in 3D Collagen

(A) Schematic illustration of the HIV-iGFP/dTomato reporter vector. PR, protease cleavage site.

(B) Immature or LPS-stimulated MDDCs were incubated with HIV-iGFP/dTomato for the indicated times and viral capture kinetics assessed by flow cytometry. Numbers indicate % of DCs that captured HIV-iGFP particles.

(C) Time course analysis of HIV-iGFP capture by DC populations. Representative data from two (immature DC) and three (mature DC) independent experiments are shown. Mean ± SEM.

(D) A time series micrograph of immature or LPS-stimulated DCs exposed to HIV-iGFP in collagen for the indicated times. Time stamp in min:sec represents elapsed time of the recordings and not the start of HIV incubation. Right panels: 3D surface rendering of DCs and HIV particles, with XY, YZ, and XZ views that illustrate viral particle distribution.

(E) Representative line profile analysis of GFP fluorescence intensity in HIV-captured DC, from the leading to the trailing edge of each cell. Representative "HIV capture" and "HIV compartmentalization" line profiles are shown. HIV compartmentalization was defined as >70% of total GFP fluorescence that is confined within the training edge of polarized DCs. Relative proportion of HIV found compartmentalized over time is shown. Data from two independent experiments are shown (n = 303 total cells).

and retain HIV within clusters that seem to polarize toward the trailing edge, or uropodia, of motile DCs within a 3D environment.

HIV Clusters within CD81-Rich Compartments near the Uropodia of Motile DCs

To better define the HIV-containing compartment, HIV-containing DCs (1 h virus pulse) were labeled with fluorophore-conjugated antibodies recognizing the uropodial marker P-selectin glycoproptein-1 (PSGL-1) or CD81 prior to collagen embedding for live-cell imaging. We observed strong co-localization between HIV clusters and both PSGL-1 and CD81, but not with dextran-containing endosomes, confirming that virus-containing compartments (VCCs) are distinct from endosomes (Figures 2A and 2B). Ultrastructural analysis using electron microscopy of HIV-captured DCs in collagen confirmed that mature viral particles were contained close to the cell surface membrane within invaginated pockets (Figures 2E and S3). These data confirm that the observed GFP + clusters in DCs were indeed mature HIV particles and not endocytosed free Gag-iGFP proteins. We observed some DCs that had more than one irregularly shaped VCCs near the uropodia containing mostly mature HIV, and no viral budding events in this compartment was observed in our analysis. Menanger and Littman (2016) showed that dynamin-2, a regulator of actin polymerization, helped facilitate the formation of HIV-containing compartments within DCs. Indeed, pre-treatment of DCs with Dynasore, a reversible inhibitor of dynamin, did not interfere with HIV capture but resulted in a complete loss of viral cluster polarization and migration (Figure 2C and Video S2). Phalloidin staining of formalin-fixed, Dynasore-treated DCs in collagen, which preserved the dendritic features of motile DCs, confirmed lower F-actin content and increased endocytosis of HIV particles (Figure 2D). When Dynasore was removed from the cell suspension by media wash after 2 h of drug treatment, DC motility and virus compartmentalization was restored, supporting the notion that actin networks are crucial for VCC maintenance in motile DCs.

Siglec-1 Facilitates HIV Compartmentalization in Motile DCs

Previous studies (Akiyama et al., 2015; Izquierdo-Useros et al., 2012a, 2012b, 2014; Perez-Zsolt et al., 2019) showed that Siglec-1 (CD169) was largely responsible for HIV capture by DCs in a gp120-independent manner. Indeed, wild-type and HIV-iGag*ΔEnv* were captured with equal efficiencies and compartmentalized by DCs near the uropodia (Figure 3A). As Siglec-1 is upregulated in mature MDDCs (Figure 3B), we further confirmed that Siglec-1 was the predominant receptor that facilitated HIV capture, as blockade with anti-Siglec-1 antibody (at a titrated dose that yielded ~90% receptor blockade) led to near-complete reduction of both wild-type and HIV*ΔEnv* capture and retention (Figures 3C and 3D). This was also confirmed by immunostaining in collagen gels, where wild-type and HIV*ΔEnv* both co-localized with Siglec-1 at the uropodia of migrating DCs (Figures 3E and 3F). Conversely, blockade with anti-DC-SIGN did not lead to significant reduction in HIV capture (Figure S4B), although DCs did express the receptor. DC-SIGN expression did not co-localize with viral clusters near the uropodia of polarized DCs in collagen (Figures S4B and S4C), indicating that DC-SIGN played a minimal role in viral capture in our model. Notably, Siglec-1 expression in control DCs were not localized exclusively in the uropodia, suggesting that HIV-binding caused HIV:Siglec-1 clusters to relocate toward the uropodia.

HIV-Captured DCs Retain Migration toward Lymph Node Homing Chemokines

Mucosal DCs capture antigens and actively migrate to the draining lymph node via the afferent lymphatics (Martín-Fontecha et al., 2009; Permanyer et al., 2018; Platt and Randolph, 2013; Randolph et al., 2005). Although HIV-captured DCs appear to retain their baseline motility, albeit at a lower velocity (Figure S1),

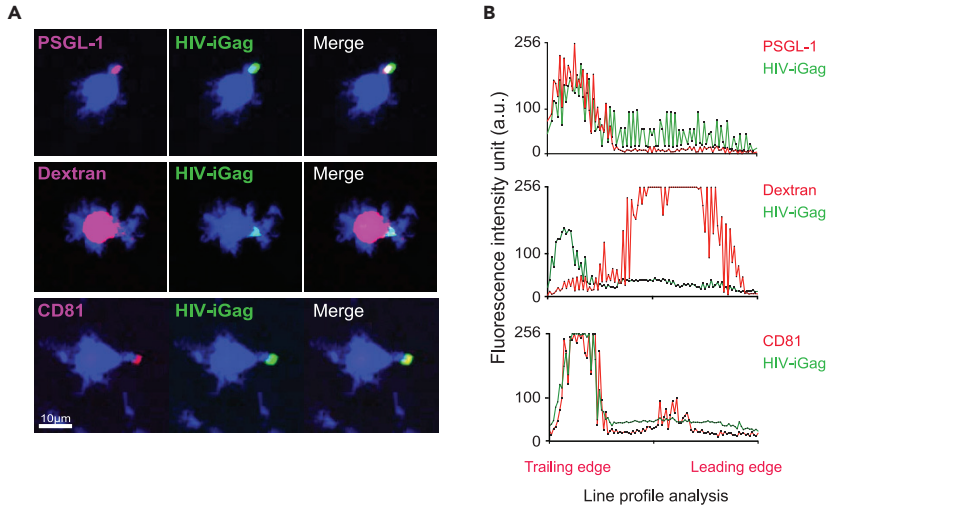
A
PSGL-1
HIV-iGag
Merge
Dextran
HIV-iGag
Merge
CD81
HIV-iGag
Merge
10μm
B
Fluorescence intensity unit (a.u.)
256
100
0
PSGL-1
HIV-iGag
Dextran
HIV-iGag
CD81
HIV-iGag
Trailing edge
Leading edge
Line profile analysis

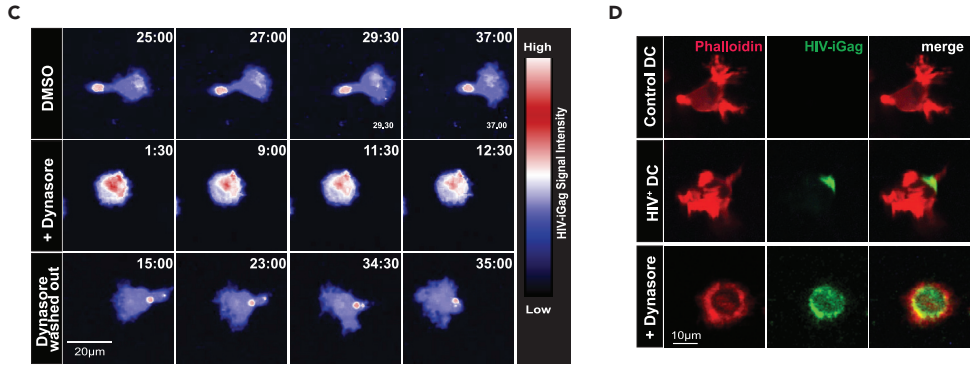
C
DMSO
25:00
27:00
29:30
37:00
+ Dynasore
1:30
9:00
11:30
12:30
Dynasore washed out
15:00
23:00
34:30
35:00
20μm
High
HIV-iGag Signal Intensity
Low
D
Control DC
HIV+ DC
+ Dynasore
Phalloidin
HIV-iGag
merge
10μm

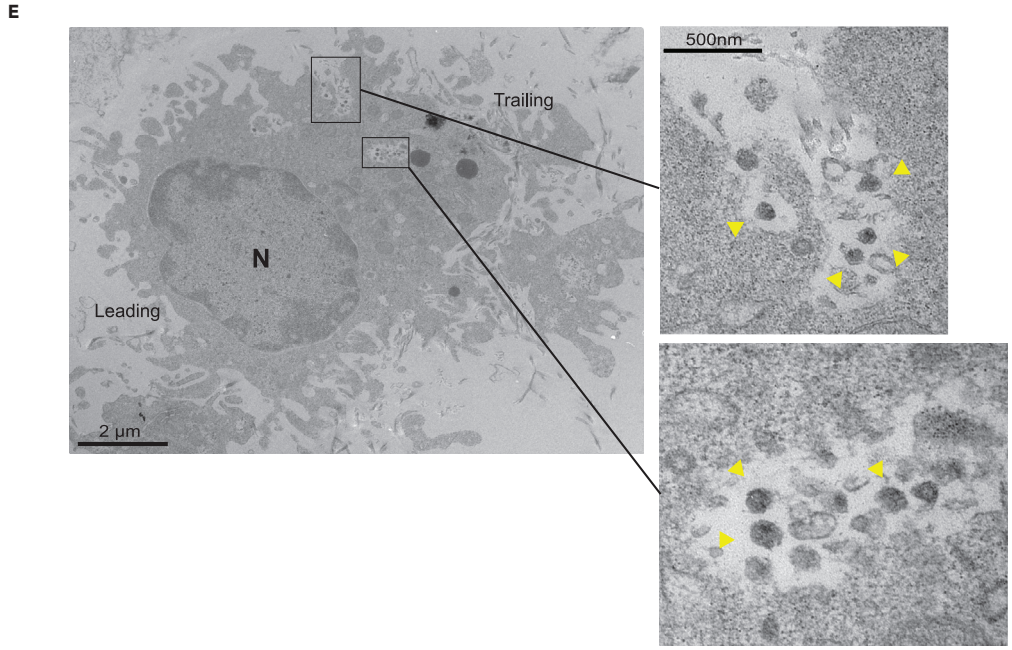
E
Trailing
N
Leading
2 μm
500nm

Figure 2. HIV Capture Kinetics and Localization by Mature DCs in 3D Collagen

(A) Micrograph of mature DCs stained for PSGL-1, CD81 or pulsed with fluorescently labeled dextran after pulsing with HIV particles for 1 h. DCs were embedded into collagen matrix for live-cell imaging.

(B) Representative life profile analysis of GFP and PSGL-1, dextran or CD81 fluorescent intensity in a polarized, HIV-captured DC (n = 33 total cells). Fluorescence intensity is expressed as arbitrary units (a.u.).

(C) Time-lapse micrograph of HIV-captured DCs that were either left alone or treated with Dynasore and prepared for live-cell imaging in collagen matrix. HIV-iGFP signal intensity is depicted using LUT union Jack analysis. Dynasore "wash out" condition involved washing DCs with media after 2 h of drug treatment.

(D) HIV-captured DCs were either left alone or treated with Dynasore, then embedded in collagen and fixed with PFA *in situ* at 37°C. DCs were stained with phalloidin-Texas red. Representative micrograph of HIV-captured DCs are shown.

(E) Transmission electron micrograph of a polarized DC in collagen matrix. HIV particles are observed within surface-accessible compartments (yellow arrowheads in enlarged insets). The leading and training edges are indicated, based on the location of the nucleus (N).

we addressed whether virus capture altered their migration toward tissue exit chemo-attractants CCL19/21 and S_1P. No changes in their respective receptors CCR7 or S_1PR1 on DCs before and after HIV exposure was observed, and comparable chemotactic responses toward CCL19/21 and S_1P gradients were noted between the two DC populations (Figures 4A and 4B). Chemotactic responses of HIV-captured DCs were significantly reduced by anti-CCR7 antibody and FTY720 treatment that blocks CCR7- and S_1PR1-mediated chemotaxis, respectively. We next addressed whether HIV-captured DCs were able to enter and migrate within lymphatic vessels, a critical step for active dissemination into the lymph node. We utilized an *ex vivo* explant model of the murine ear dermis, taking advantage of the fact that human immune cells responded robustly to murine CCL19/21 (Deruaz et al., 2017). Lymphatic vessels from mouse explants were labeled using anti-LYVE-1 antibody, then a 1:1 mixture of control and HIV-captured DCs were overlaid for 15 min to allow for cells to enter the dermal layers of the skin for microscopy analysis (Figure 4C). We found equal proportions of control and HIV^+ DCs within lymphatic vessels and dermal interstitium, demonstrating that DCs suffered no defect in lymphatic entry after HIV capture (Figure 4D). Pre-treatment of DCs with anti-CCR7 antibody and FTY720 (an S_1PR1 antagonist) resulted in a shift in DC proportions from the lymphatic vessels to the interstitial space, compared with vehicle-treated cells (Figure 4E). Notably, CCR7/S_1PR1 dual blockade led to non-linear motility toward the nearest lymphatic vessel and a more tortuous DC migration pattern, showing loss of directionality (Figures 4F and 4G). Together, HIV capture and compartmentalization in DCs did not abrogate their chemotactic responses toward tissue exit signals, and both CCR7 and S_1PR1 enabled DC entry and intraluminal crawling within lymphatic vessels (Figure 4H and Video S3).

Prolonged DC:T Cell Engagement Is Facilitated through gp120:CD4 Interaction

Mature DCs migrate into and within the T cell zone of the lymph node to maximize access to naive T cells (Mempel et al., 2004; Miller et al., 2003). Virological synapse (VS) formation between HIV-infected and uninfected cells are well described and serve as a direct conduit for efficient HIV spread to susceptible T cells (Jolly et al., 2004; Jolly and Sattentau, 2004). We next sought to visually characterize the cellular dynamics during DC:T cell *trans*-infection within a fibrillar 3D environment that allows cells to migrate, locate, and engage other cells in a manner that are reflective of interactions observed in the LN. Activated $CD4^+$ T cells were co-cultured with either HIV-captured DCs or cell-free HIV particles in collagen matrices for 4 h, after which T cells were isolated and incubated in fresh media for an additional 48 h to measure productive, dTomato expression (Figure 5A). The presence of DCs significantly increased T cell infection compared with cell-free virus alone, and raltegravir pre-treatment completely inhibited infection in both experimental conditions. Next, we addressed how physiological DC:T cell contact dynamics were impacted upon HIV exposure using live-cell microscopy. As expected, DC:T cell contacts in the absence of infection remained brief, with mean durations lasting under 5 min, whereas extended DC:T cell contacts (mean duration of ~17 min) were observed in the presence of HIV particles (Figures 5B and 5C and Video S4). When DC:T cell contact durations were further characterized as brief (<5 min), scanning (5–17 min), or stable (>17 min), we noted that more than 70% of all DC:T cell conjugates were either scanning or stable contacts in the presence of virus (Figure 5D), indicating a substantial increase in DC:T cell dwell times. Surprisingly, stable DC:T cell contacts were completely abrogated in the presence of HIV-iGag*ΔEnv*, suggesting that gp120:CD4 interactions facilitate durable DC:T cell contacts. Similar reductions in DC:T cell contact duration was observed after CD4 antibody blockade (Figures 5C and 5D). Since HIV-captured DCs were not productively infected and did not express *de novo* gp120 on the cell surface, we interpreted these data as surface-accessible Siglec-1:HIV complexes functioning as adhesive molecules to retain motile

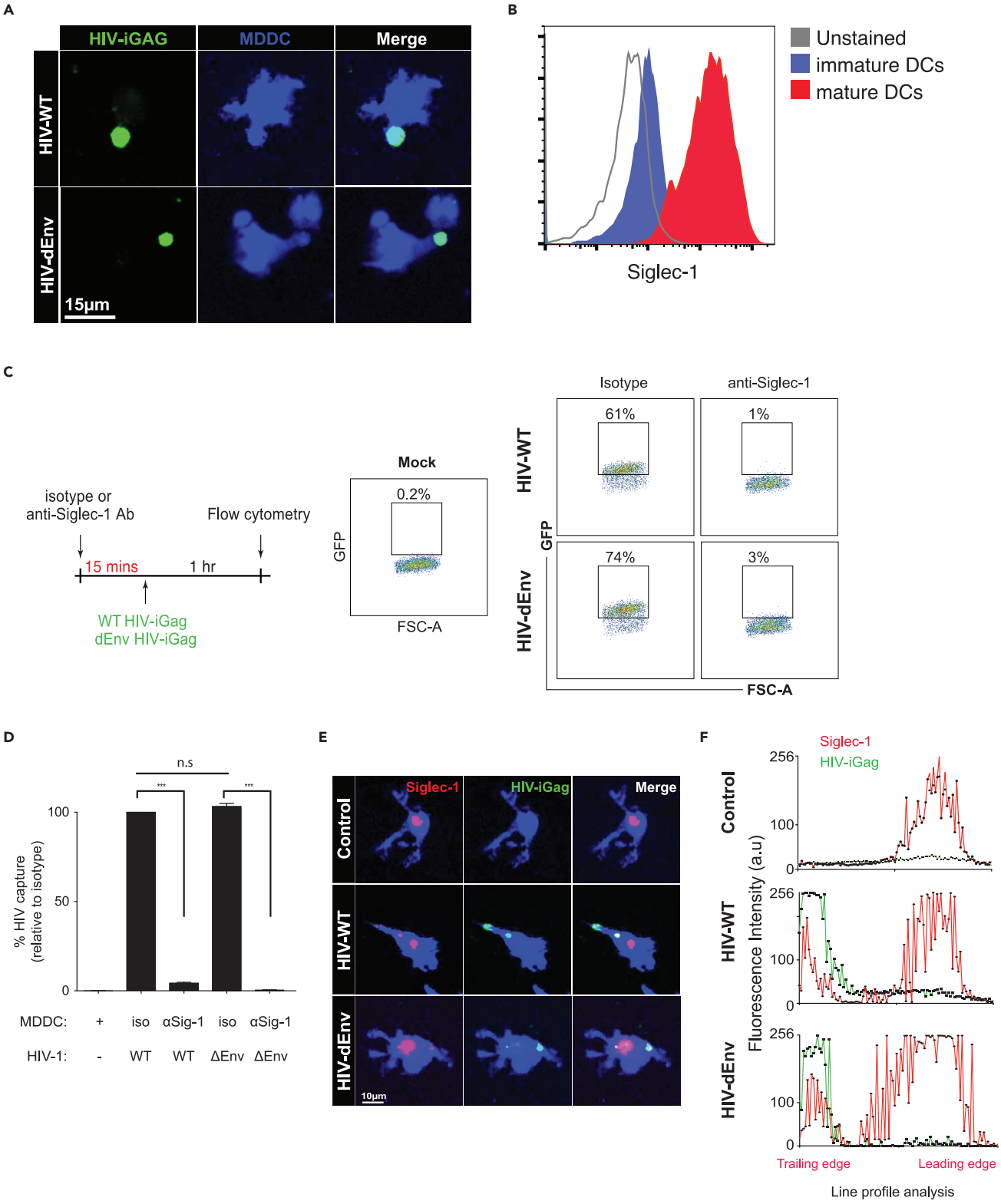

Figure 3. Siglec-1 Mediates HIV Capture and Uropodial Compartmentalization in Motile DCs

(A) Micrograph of mature DCs pulsed with either wild-type or *ΔEnv* HIV-iGFP, washed, and embedded in collagen for live-cell imaging. Time stamp: min:sec.

(B) Expression of cell surface Siglec-1 on mature DCs.

Figure 3. *Continued*

(C) DCs were treated with either isotype or anti-Siglec-1 antibody prior to exposure to wild-type or *ΔEnv*HIV-iGFP. Numbers indicate % of DCs that captured HIV particles.

(D) Percent HIV capture by DCs. Data was normalized to isotype antibody-treated cells. Mean ± SEM are shown. Representative data from four independent experiments are shown. n.s., not significant; ***p < 0.001. Unpaired Student's t test.

(E) Micrograph of HIV-captured DCs stained for Siglec-1 in collagen.

(F) Representative line profile analysis of GFP and Siglec-1 fluorescent intensity in a polarized, HIV-captured DC shown in (E). Representative data from three independent experiments are shown.

T cells as they scan the DC surface. Indeed, T cells contacting control DCs or Env-deficient virus-containing DCs did not decelerate during contacts, whereas a substantial reduction in scanning speeds was observed in T cells contacting HIV-captured DCs (Figures 5E–5G). These data suggest that surface-accessible HIV particles may function as adhesive molecules to "slow" T cell migration, prolonging DC:T cell contact times to enhance cell-cell HIV spread.

gp120:CD4 Binding Induces Signaling that Further Stabilizes DC:T Cell Interactions

We postulated that repeated gp120:CD4 interactions during T cell scanning of the DC surface may invoke signals that promote stable DC:T cell conjugates. Previous studies have demonstrated that gp120:CD4 engagement induces phosphorylation of Lck, TCRζ chain, and AKT and induces T cell stop (Hioe et al., 2011; Vasiliver-Shamis et al., 2008, 2009). Since LFA-1:ICAM-1 adhesive contacts are also an essential facilitator of DC *trans*-infection (Hioe et al., 2011; Wang et al., 2009), we tested whether Siglec-bound HIV can regulate LFA-1 activation in scanning T cells. Using a monoclonal antibody that binds to high affinity confirmation LFA-1 (clone 24) (Laufer et al., 2018), a measurable increase in high affinity LFA-1 was observed in T cells after co-culture with wild-type HIV-pulsed DCs, but not with control or HIV-iGag*ΔEnv*-pulsed DCs, suggesting that gp120-mediated modulation of T cell migration was at least partially dependent on LFA-1 activation (Figure 6A). Blocking LFA-1:ICAM-1 interactions resulted in a substantial reduction in stable DC:T cell contacts and lower T cell infection, supporting their role in cell-cell stabilization and viral transmission (Figures 6B–6D). To further identify signaling networks activated by gp120:CD4 interactions, T cells were co-cultured with DCs pulsed with either wild-type or HIV-iGag*ΔEnv*, harvested after 15 min and analyzed for signaling networks using a custom human peptide kinome array (Nickol et al., 2019). Ingenuity pathway analysis (IPA) identified upregulation of the PI3K pathway, calcium signaling, and ERK/MAPK pathways in T cells, among others, during contacts with wild-type, but not HIV-iGag*ΔEnv*-captured DCs (Figure 6E and Table S1). InnateDB analysis also predicted upregulation of "TCR signaling," "MAPK pathways," and "Focal adhesions" (Table S2), identifying signaling pathways that are initiated through Env:CD4 engagement.

DISCUSSION

During vaginal transmission, HIV establishes a focal infection within the CVT, which disseminates to draining and distant lymphoid organs prior to viral detection in blood. In order for HIV to establish a persistent infection, it needs to replicate quickly and find new target cells in the face of increasing adaptive immune pressure. It is now well documented that HIV takes advantage of the physiological trafficking properties of immune cells to gain access to large numbers of target T cells and that these mechanisms are particularly important during the early stages of transmission (Deruaz et al., 2017; Fackler et al., 2014; Murooka and Mempel, 2012; Pena-Cruz et al., 2018; Usmani et al., 2019). DCs can enhance viral spread in cultures (Cameron et al., 1992), but insights into cellular dynamics that orchestrate DC-to-T cell viral dissemination using experimental models that allow cells to migrate, locate, and engage each other are still lacking. The main question we addressed in this study is how HIV-captured DCs, which do not express *de novo* Env on the cell surface, regulate T cell behaviors in the absence of cognate antigen recognition. Herein, we have mapped key mechanisms of how migratory DCs capture, transport, and transmit infectious HIV to susceptible T cells and demonstrate that surface accessible Siglec:HIV clusters act as adhesive/signaling receptors to form a crucial contact point with scanning T cells. This in turn leads to gp120-mediated activation of LFA-1 and signal transduction that induces T cell stop and activation to promote high viral spread. Thus, we describe a mechanism by which a relatively small number of HIV-captured DCs, in the absence of infection, can ignite exponential T cell infection using a previously unknown mechanism of restraining motile T cells to maximize viral spread efficiency.

DCs act as tissue sentinels throughout the body, including the female genital tract (FGT) (Lindquist et al., 2004; Satpathy et al., 2012). The presence of microbial products and inflammatory stimuli leads to their

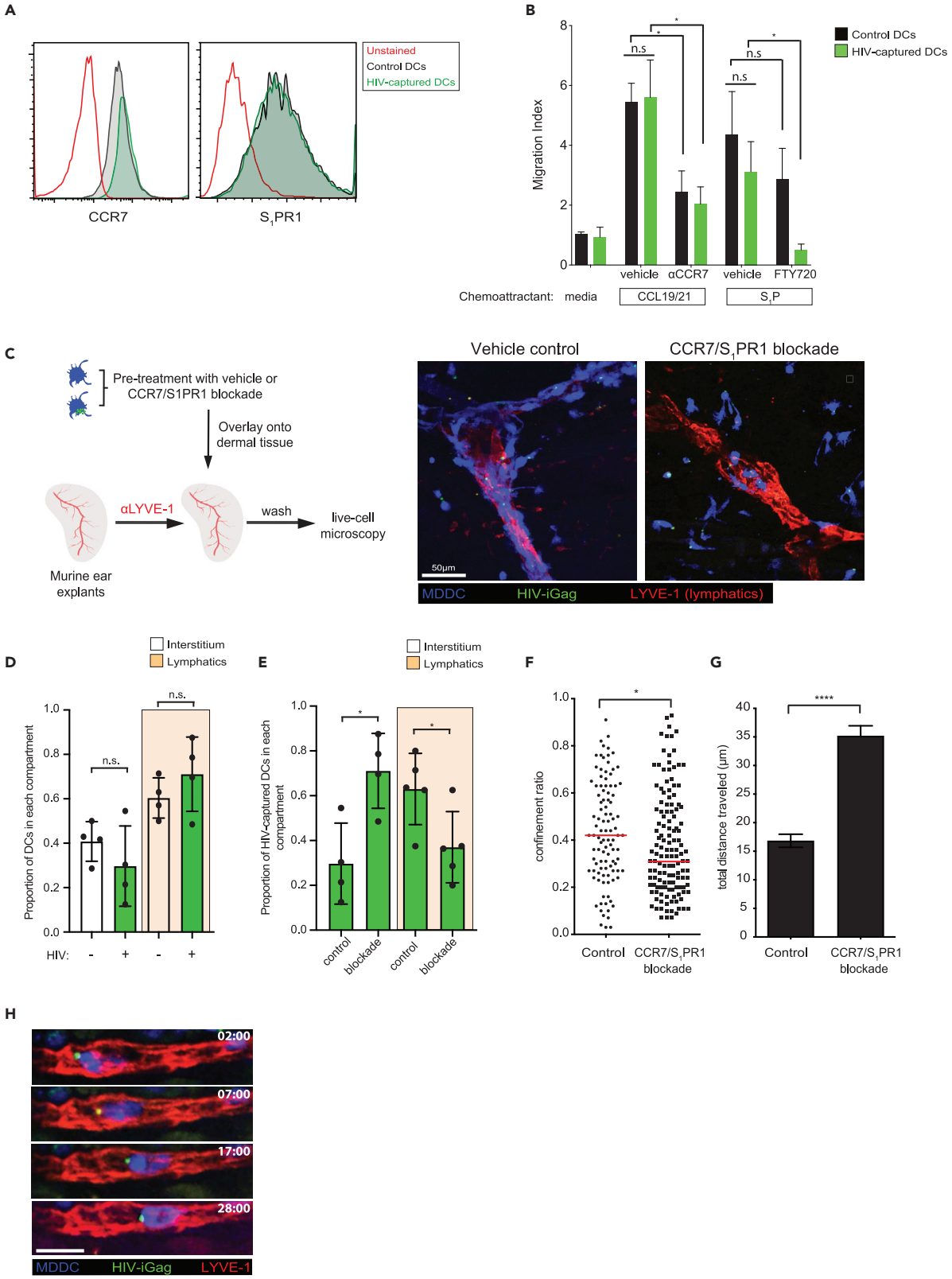
A
Unstained
Control DCs
HIV-captured DCs
CCR7
S1PR1
B
Migration Index
Control DCs
HIV-captured DCs
n.s
vehicle
αCCR7
vehicle
FTY720
Chemoattractant: media
CCL19/21
S1P
C
Pre-treatment with vehicle or CCR7/S1PR1 blockade
Overlay onto dermal tissue
αLYVE-1
wash
live-cell microscopy
Murine ear explants
Vehicle control
CCR7/S1PR1 blockade
50μm
MDDC
HIV-iGag
LYVE-1 (lymphatics)
D
Interstitium
Lymphatics
Proportion of DCs in each compartment
n.s.
HIV:
E
Proportion of HIV-captured DCs in each compartment
control
blockade
F
confinement ratio
Control
CCR7/S1PR1 blockade
G
total distance traveled (μm)
****
H
02:00
07:00
17:00
28:00
MDDC
HIV-iGag
LYVE-1

Figure 4. HIV-Captured DCs Display Robust Migration and Lymphatic Vessel Entry

(A) Cell surface expression of CCR7 and S_1PR1 on control or HIV-captured DCs.

(B) Transwell migration analysis of control or HIV-captured DCs in response to media, CCL19/21, or S_1P. In some conditions, DCs were pre-treated with anti-CCR7 blocking antibody or FTY720-P before subjecting them to the migration assay. Migration index was calculated as fold increase in the number of DCs that responded to chemokine compared with media alone. Mean chemotactic responses +/− SEM toward CCL19/21 and S_1P from three and two independent experiments, respectively, are presented. *$p < 0.05$, Mann-Whitney U test.

(C) Experimental design of the *ex vivo* skin crawl-in assay. A mixture of control and HIV-captured DCs (1:1) were pre-treated either with vehicle or with both anti-CCR7 antibody and FTY720-P, washed, and overlaid on dermal tissue. Cells that did not enter the tissue were washed and prepared for live-cell imaging. Right panel: representative micrograph of control and HIV-captured DC distributions in the presence or absence of chemokine receptor blockade.

(D) Relative distribution of control or HIV-captured DCs within the visualized dermal lymphatics or interstitium compartment. Mean values from four independent experiments +/− SEM are shown. n.s., not significant, chi-square test.

(E) Relative distribution of HIV-captured DCs before and after chemokine receptor blockade with the visualized dermal lymphatics or interstitium. *$p < 0.05$, chi-square test.

(F) Confinement ratio within the dermal skin layer before or after receptor blockade. Unpaired Student's t test was performed. n.s., not significant. ****$p < 0.001$. Confinement ratio is defined as the ratio of the displacement of a cell to the total length of the path the cell has traveled. Data from four independent experiments are shown. Mean ± SEM are shown.

(G) Total displacement of DCs within the dermal skin layer before or after receptor blockade. Mann-Whitney U test was performed. n.s., not significant. ****$p < 0.001$. Data from four independent experiments are shown. Mean ± SEM are shown.

(H) Time-lapse micrograph of an HIV-captured DC undergoing intraluminal crawling. Scale bar, 20μm.

maturation and upregulation of chemokine receptors that help direct their migration into secondary lymphoid organs, where a single DC will interact with up to 5,000 T cells per hour (Bousso and Robey, 2003; Miller et al., 2004). Upon cognate antigen recognition, prolonged DC:T cell interactions dictate the magnitude of T cell differentiation, effector function, and memory responses (Henrickson et al., 2008; Mempel et al., 2004). Although migratory DCs are less susceptible to productive HIV infection due to high expression of the restriction factor SAMHDI (Laguette et al., 2011), their ability to capture (Bertram et al., 2019) and transmit viral particles to T cells at the site of cell-cell contact, known as *trans*-infection, has implications on their ability to drive systemic dissemination after mucosal viral exposure (Cavrois et al., 2007; Izquierdo-Useros et al., 2007; McDonald et al., 2003; Yu et al., 2008). We previously showed that blocking leukocyte trafficking with the S_1PR1 antagonist FTY720 or pertussis toxin, which inhibits G-protein-coupled receptors, substantially limited viral spread to peripheral tissue sites after vaginal HIV challenge of humanized mice (Deruaz et al., 2017). To further extend these observations, we focused on the role of migratory DCs in this process and show that HIV-captured DCs retain their ability to migrate toward lymph node-homing chemo-attractants S_1P and CCL19/21 and that their cognate receptor expression remains unchanged upon virus capture. Since murine S_1P and CCL19/21 were functional on human cells, we took advantage of an *in situ* skin crawl-in assay to demonstrate that HIV-captured DCs displayed directional, haptotactic guidance toward the lymphatic vessel, followed by entry and intraluminal crawling under the influence of endogenous chemokine gradients. S_1PR1/CCR7 dual blockade resulted in reduced DC accumulation near lymphatic vessels and displayed a more tenuous migratory path, indicating loss of directionality. These observations are supported by the role of CCR7 and S_1PR1 in leukocyte egress from peripheral tissues into afferent lymphatics and LNs at homeostasis (Bromley et al., 2005; Czeloth et al., 2005; Debes et al., 2005; Forster et al., 1999; Gollmann et al., 2008; Idzko et al., 2002; Lan et al., 2005, 2008; Russo et al., 2016; Tal et al., 2011; Weber et al., 2013) and during inflammation (Brown et al., 2010). Following lymphatic entry, DCs crawl on endothelial cells in the direction of lymph flow, but they get passively transported with the lymph once they reach collecting lymphatics (Girard and Springer, 1995; Tal et al., 2011). Notably, FTY720 treatment was more effective in suppressing viremia compared with CCR7 blockade after vaginal HIV exposure in humanized mice, suggesting that S_1PR1 may play a dominant role in regulating DC egress. However, we cannot completely rule out the possibility that the CCR7 pathway might contribute to egress of other infected or HIV-containing cell types into peripheral tissues.

Siglec-1 is expressed in cervical $CD14^+CD11c^+HLA\text{-}DR^+$ DCs and MDDCs and has been implicated in HIV capture and retention that is dependent on ganglioside GM3 binding and not HIV gp120 (Crocker et al., 2007; Gummuluru et al., 2014; Izquierdo-Useros et al., 2012a, 2012b, 2014; Perez-Zsolt et al., 2019). This was confirmed in our study, as dense clusters of wild-type and Env-deficient HIV both co-localized with Siglec-1 near the DC uropodia. Ultrastructural analysis by TEM confirmed the presence of mature HIV particles within surface-accessible virus containing compartments (VCCs) and membrane invaginations near the rear end of polarized DCs. The observed HIV clusters also co-localized with $CD81^+$ but were distinct from endosomes, consistent with previous characterizations of these non-lysosomal compartments in mature DCs (Gummuluru et al., 2014). It is likely that endocytosed HIV particles are rapidly degraded by

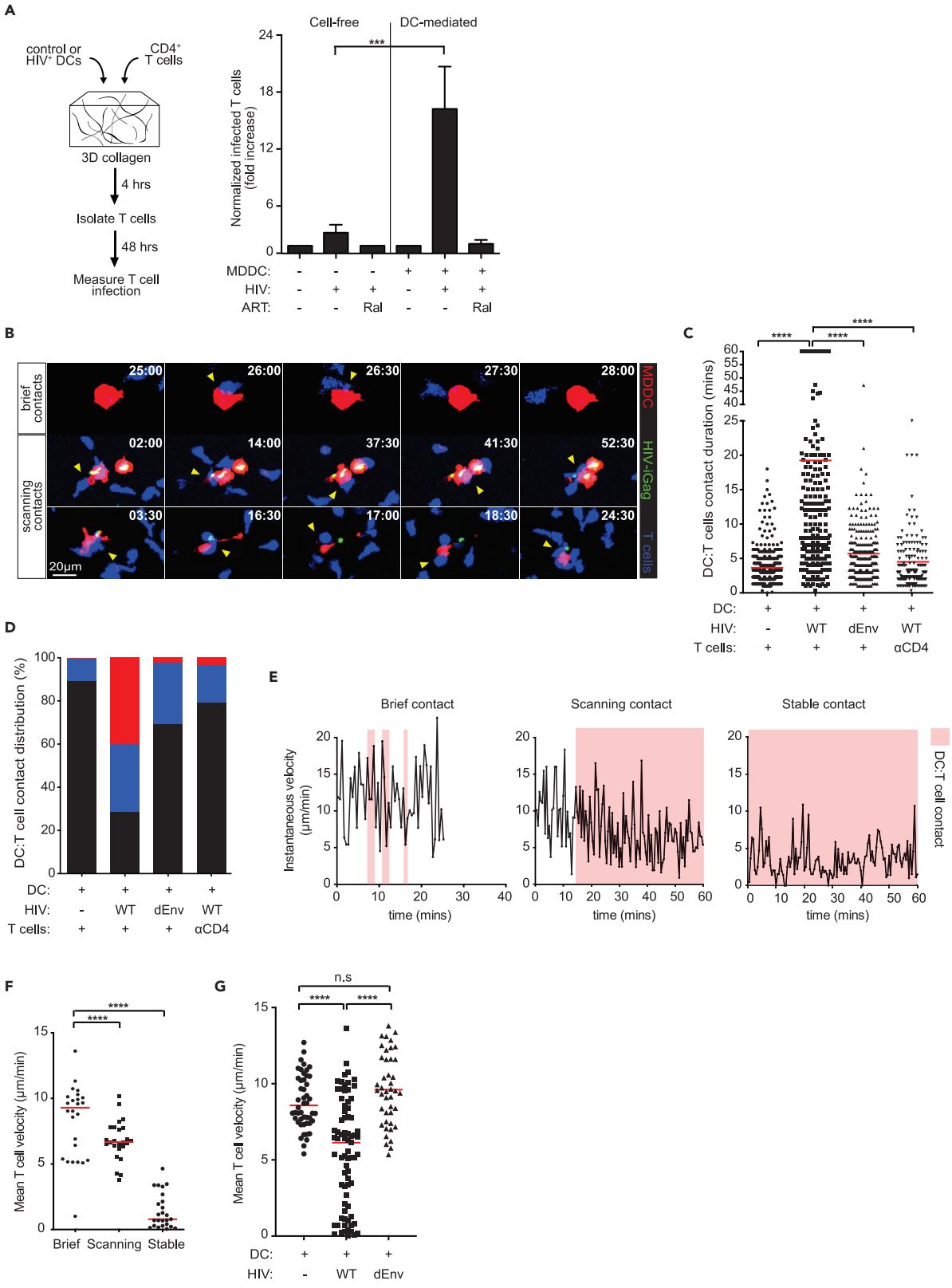
A
control or HIV+ DCs
CD4+ T cells
3D collagen
4 hrs
Isolate T cells
48 hrs
Measure T cell infection
Cell-free
DC-mediated
***
Normalized infected T cells (fold increase)
MDDC:
HIV:
ART:
Ral
B
brief contacts
scanning contacts
25:00
26:00
26:30
27:30
28:00
02:00
14:00
37:30
41:30
52:30
03:30
16:30
17:00
18:30
24:30
20μm
MDDC
HIV-iGag
T cells
C
DC:T cells contact duration (mins)
****
DC:
HIV:
T cells:
WT
dEnv
αCD4
D
DC:T cell contact distribution (%)
E
Brief contact
Scanning contact
Stable contact
Instantaneous velocity (μm/min)
time (mins)
DC:T cell contact
F
Mean T cell velocity (μm/min)
Brief
Scanning
Stable
G
n.s

Figure 5. HIV-Captured DCs Engage in Prolonged Contacts with T Cells in a gp120:CD4-Dependent Manner

(A) Control or HIV-captured DCs were co-cultured with T cells and embedded into a collagen matrix for 4 h. T cells were extracted after collagenase treatment and incubated for an additional 48 h to measure productive infection. Normalized fold increase in T cell infection in the indicated conditions are shown. Data are from three independent experiments. Mean ± SEM are shown. Ral, raltegravir. ***p < 0.01, Unpaired Student's t test.

(B) Time-lapse micrographs of DC:T cell contacts that are defined as brief or prolonged interactions. Time stamp are in min:sec of the movie recordings.

(C) DC:T cell contact duration in the presence of wild-type or HIV-iGFP*ΔEnv*. Red lines indicate median values. αCD4, anti-CD4 antibody. ****p < 0.001, Mann-Whitney U test. Data from ten independent experiments are shown (n = 1,172 total DC:T cell contact events).

(D) Percent distribution of DC:T cell contact times defined as brief (>7 min; black), prolonged (7–17 min; blue), or stable (>17 min; red) are shown.

(E) Representative of instantaneous speeds of a T cell during a brief, prolonged, or stable contact with a DC is shown. Red shaded area represents a DC-T cell contact event. Data from two independent experiments are shown (n = 3 of total DC:T cell contact events).

(F) Mean T cell velocity during brief, prolonged, or stable contacts with HIV-captured DCs. Red lines indicate median values. Data from three independent experiments are shown (n = 75 total cells). ****p < 0.001, Mann-Whitney U test.

(G) Mean T cell velocity during contact with control, wild-type HIV, or HIV-iGag*ΔEnv*-pulsed DCs. Mean velocity was defined as the average speeds of a single T cell track contacting a DC. Red lines indicate median values. Data from three independent experiments are shown (n = 171 total cells). ns, not significant. ****p < 0.001, Mann-Whitney U test.

phagolysosomes for antigen presentation, whereas those that are contained within Siglec-1^{+}CD81^{+} compartments remain intact for up to 24 h, based on high HIV-GFP retention in our studies. Retained HIV particles can then access target CD4+ T cells through DC:T cell interactions in a way that is analogous to the capture of ganglioside-rich exosomes by mDCs and amplification of the immune response without antigen reprocessing (Izquierdo-Useros et al., 2014; Nasr et al., 2014). Subcapsular sinus (SCS) macrophages also express Siglec-1 (CD169) (Asano et al., 2011; Edgar et al., 2019; Grabowska et al., 2018; Hammonds et al., 2017; Junt et al., 2007; Saunderson et al., 2014; Uchil et al., 2018) that play a vital role in pathogen capture and transport to DCs or the B cell follicles (Grabowska et al., 2018; Phan et al., 2009; Veninga et al., 2015). HIV and MLV (murine leukemia virus) have been shown to exploit SCS macrophages to access target CD4 T cells and B cells, respectively, and facilitate efficient viral spread *in vivo* (Sewald et al., 2015). In our study, Siglec-1 was rarely found near the uropodia in control DCs, whereas dense HIV:Siglec-1 clusters localized near the trailing edge shortly after HIV exposure. How HIV:Siglec-1 relocates near the uropodia is not clear, as Siglec-1 lacks tyrosine-based signaling motifs and the cytoplasmic tail is poorly conserved compared with others in the Siglec family (Crocker et al., 2007). However, the uropodia of migrating cells is a specialized platform for organelles, adhesion receptors, and key regulators of the actin polymerization machinery, suggesting that HIV:Siglec-1 clusters may be actively transported to the uropodia rather than passive accumulation. The trailing edge is also enriched with tetraspanin-containing microdomains that are crucial for the formation of VCCs (Barreiro et al., 2008; Suárez et al., 2018). Interestingly, the uropodia of polarized T cells has been shown as the preferred site for membrane-associated Gag accumulation and VS formation (Hatch et al., 2013). Together, Siglec-1-mediated HIV capture and retention occur highly localized within the uropodia of migrating DCs, but within compartments that are accessible by T cells during DC:T cell interactions.

Two-photon microscopy analyses have revealed that naive T cells crawl along the surface of the FRC network in an apparently random manner and continually scan dendritic cells that are also situated on the same FRC networks, in search for cognate antigen (Mempel et al., 2004; Miller et al., 2003). These studies have forced us to re-evaluate the interplay between cell motility, cell-cell contact dynamics, and *trans*-infection mechanisms, where dynamic DC:T cell interactions occur continuously. We performed live-cell imaging studies in collagen matrices to visually characterize how HIV-containing DCs alter the speed and duration of T cell scanning behaviors in a fibrillar 3D setting that better reflect their physiological interactions *in vivo*. High T cell infection rates were observed in the presence of DCs in collagen compared with free-virus alone, and this corresponded with a high proportion of stable DC:T cell contacts. Interestingly, we observed that stable DC:T cell conjugates were abrogated in the presence of Env-deficient HIV, or after CD4 antibody blockade, despite similar viral capture kinetics and localization to wild-type HIV. These data seemed to suggest that the presence of virus-containing invaginations modulated T cell scanning and migration and that this involved Env:CD4 interactions. Elegant ultrastructural analysis of the DC:T cell conjugate site has revealed T cell-derived filopodial protrusions that penetrate into the virion-rich folds of dendritic cells and attachment of viral particles along these actin-rich extensions (Felts et al., 2010). Addition of blocking antibodies against gp120 resulted in retention of virions by dendritic cells, whereas CD4 antibody blockade prevented DC-to-T cell viral transmission. Together, these data illustrate a scenario where actively scanning T cells probe the DC surface with CD4-rich filopodial protrusions, which upon contact with HIV clusters embedded within membrane invaginations, leads to generation of signals that culminate in T cell arrest and VS formation in a gp120:CD4-dependent manner. Our observations that T cells appear either arrested

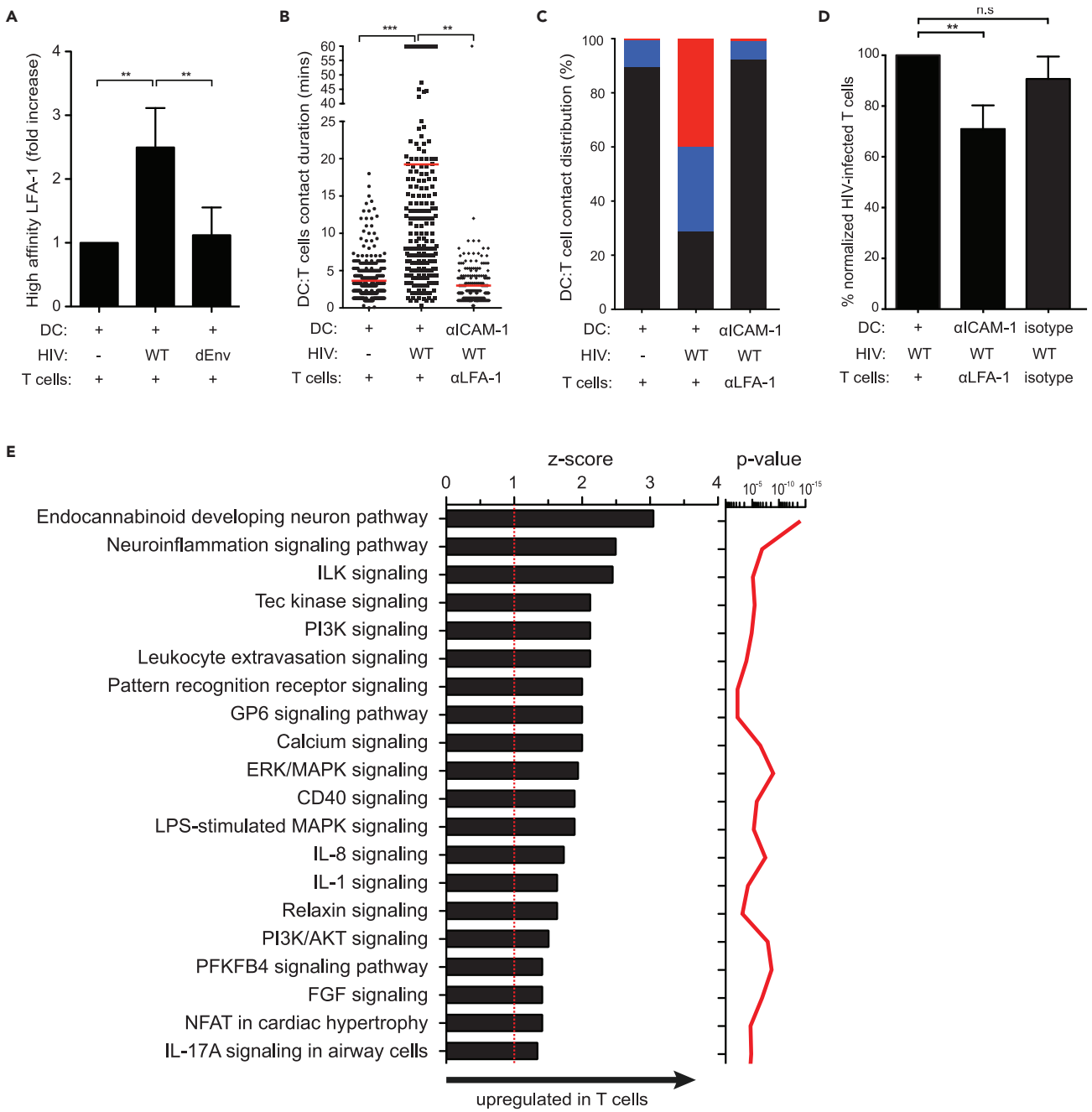

Figure 6. LFA-1:ICAM-1 Binding Stabilizes Stable DC:T Cell Contacts and Facilitates Viral Transmission

(A) Flow cytometry analysis of high-affinity LFA-1 expression (mAb clone 24) on T cells after co-culture with HIV-captured DCs. Data are normalized to no virus DC:T cell controls. Data from two healthy donors. Mean ± SEM are shown. **$p < 0.01$, Unpaired Student's t test.

(B) DC:T cell contact duration in the presence or absence of LFA-1:ICAM-1 interactions. ICAM-1, anti-ICAM-1 antibody; αLFA-1, anti-LFA-1 antibody. Red lines indicate median values. **$p < 0.01$, ***$p < 0.001$, Mann-Whitney U test. Data from eight independent experiments are shown (n = 957 total DC:T cell contact events).

(C) Percent distribution of DC:T cell contact times defined as brief (>7 min; black), prolonged (7–17 min; blue), or stable (>17 min; red) from data in (B) are shown.

(D) Percent normalized T cell infection with the indicated antibody blockade. Data are from two independent experiments. Mean ± SEM are shown. n.s., not significant. **$p < 0.01$, Unpaired Student's t test.

(E) IPA identified biological pathways that were significantly ($p < 0.01$) upregulated (Z score > 1) in T cells co-cultured with wild-type HIV-pulsed DCs (T cells co-cultured with HIV-iGag⊿*Env*-pulsed DCs set as background controls). The p value (red line), calculated with the Fischer's exact test, reflects the likelihood that the association between a set of activated kinases and a biological function is significant (p value ≤ 0.05).

or display low motility when contacting HIV-captured DCs, but not Env-deficient or control DCs, are in line with this model. Soluble and virion-associated gp120 can induce Ca^{2+} flux downstream of the chemokine receptors (Melar et al., 2007; Weissman et al., 1997), and calcium signaling mediates T cell arrest upon cognate antigen recognition (Bromley et al., 2000, 2001). Whether calcium signaling is required for DC:T cell conjugate formation is unclear, since gp120 molecules embedded into planar lipid bilayers arrested T cells without detectible calcium release (Vasiliver-Shamis et al., 2009). Other surface molecules can play a role in stabilizing the VS, as CD81 tetraspanin (Gousset et al., 2008), GM1 ganglioside (Jolly and Sattentau, 2005), and integrins (Jolly et al., 2004, 2007) have all been shown to accumulate at the site of cell-cell contact. Of particular importance are LFA-1:ICAM-1 adhesive interactions that facilitate VS formation (Jolly et al., 2004; Jolly et al., 2007; Rodriguez-Plata et al., 2013; Vasiliver-Shamis et al., 2010;Vasiliver-Shamis et al., 2008) and cell-cell transmission (Duncan et al., 2014; Jolly et al., 2007; Rudnicka and Schwartz, 2009). Blocking LFA1/ICAM-1 binding abrogated prolonged DC:T cell contacts in collagen and reduced T cell infection. Importantly, we found that gp120:CD4 binding was required for activation of the high-affinity conformation of LFA-1 in T cells during co-cultures with HIV^+ DCs, suggesting that HIV:CD4 binding represents an initial, critical step in facilitating prolonged DC:T cell contacts. Our data are consistent with previous studies where HIV gp120 triggered LFA-1 activation in resting CD4 T cells in a CD4-dependent manner (Hioe et al., 2011). Additionally, LFA-1 activation can also function beyond their adhesive properties to promote VS formation, as T cell polarization and MTOC reorganization toward the cell-cell contact site upon LFA-1 ligation has been reported (Starling and Jolly, 2016). Thus, our data describe a model where surface accessible HIV on DCs modulates T cell scanning behaviors by activating a gp120-dependent signaling cascade that favors stable DC:T cell contacts and viral transmission. It is unlikely that DC:T cell conjugates observed in our studies are the result of cognate antigen recognition, since T cells were isolated from healthy donors and the number of HIV-specific T cells are expected to be low. However, given that HIV-specific T cells are preferentially infected during acute infection (Douek et al., 2002; Lore et al., 2005), an intriguing question is whether antigen recognition further facilitates DC:T contacts that can simultaneously prime and transmit HIV particles to T cells, and is a focus of our ongoing studies.

HIV Env induces calcium flux, MEK/ERK activation, Lck phosphorylation, and partial ZAP-70 activation, among others, in CD4 T cells, but their role in viral entry or infection has been debated (Cicala et al., 2006; Goldman et al., 1994; Hioe et al., 2011; Juszczak et al., 1991; Melar et al., 2007; Popik et al., 1998; Vasiliver-Shamis et al., 2008, 2009). Recent studies by Lens et al. showed that Env:CD4 clustering at the site of T cell-T cell contact initiated signaling downstream of the T cell receptor in infected cells, leading to enhanced cell-cell HIV transmission (Len et al., 2017). In their study, robust signaling in target T cells were also observed, suggesting that *de novo* Env expression on infected T cells delivered activation signals during cell-cell contacts. Here, we addressed whether surface-bound HIV clusters induce similar T cell signaling pathways that modulate migratory behaviors in a way that favors viral spread. Our kinome array and IPA analysis confirmed activation of calcium signaling, TCR signaling, and ERK/MAPK pathways, among others, through Env:CD4 binding, which can collectively modulate T cell migration behaviors. Tec family of tyrosine kinases (*Z* score 2.1, p value $3.4x10^{-6}$) plays an indispensable role in T cell maturation, activation, and differentiation (Andreotti et al., 2010; Schwartzberg et al., 2005), where Itk phosphorylation downstream of the T cell receptor regulates Ca^{2+} mobilization, actin mobilization, and cytoskeletal reorganization. Previous studies have demonstrated that Itk is phosphorylated in T cells shortly after contact with gp120- and ICAM-1-embedded lipid bilayers (Vasiliver-Shamis et al., 2009) and that Itk deficiency disrupts F-actin assembly and reduces intracellular p24 levels upon HIV infection (Francois and Klotman, 2003), suggesting that this pathway may regulate both T cell motility and virus transcription. Similarly, activation of the PI3K pathway (*Z* score 2.1, p value $1.3x10^{-5}$) through gp120:CD4 interactions may regulate T cell migration behaviors and help promote HIV infection post-viral entry (Francois and Klotman, 2003; Nabel and Baltimore, 1987). Finally, the canonical MAPK/ERK pathway (*Z* score 1.9, p value $1.1x10^{-9}$) regulates cell adherence, metabolism, and cell proliferation, and inhibiting ERK signaling is known to restrain ECM-induced cell motility (Cuevas et al., 2007; Klemke et al., 1997; Krueger et al., 2001). Earlier work showed that ERK activation regulated HIV infectivity and was required for efficient organization of the reverse transcription complex (Jacque et al., 1998; Yang and Gabuzda, 1999). Activation of the Th17 signaling pathway may increase virus infection, as Th17-lineage $CCR6^+$ $CD4^+$ T cells are preferentially infected early during infection (Planas et al., 2017; Stieh et al., 2016). Together, kinome analyses suggest that DC-bound HIV can activate signaling pathways that regulate both T cell motility and viral susceptibility. Signaling activation by surface-bound HIV is not surprising, given that as little as two HIV particles were sufficient to stimulate calcium influx in primary T cells (Melar et al., 2007). Although there are a relatively low number of Env per virion

(~14 trimers) (Zhu et al., 2006), their access to CD4 molecules is augmented by the large numbers of HIV particles found within VCCs and the high frequency of serial DC:T cell interactions that occur in lymphoid organs. It is important to note that, although gp120-dependent signaling is initiated downstream of either the CD4 molecule or the CXCR4/CCR5 co-receptor, gp120:CD4 engagement is a requirement for both (Melar et al., 2007). Lck phosphorylation occurs downstream of the CD4 molecule, whereas calcium signaling is exclusively downstream of chemokine receptors, but these signals converge to regulate T cell migration behavior and function. Prior engagement of gp120 by the CD4 molecule can induce a conformational change that supports subsequent binding with the co-receptor, indicating that CD4 and co-receptor do not have to be present at the same time (Popik et al., 1998; Weissman et al., 1997). This raises an intriguing possibility that serial T cell scanning behaviors can "prime" virion-associated Env within VCCs, potentiating subsequent T cell encounters that induce a unique signaling cascade to modulate T cell motility, cell-cell adhesion, and HIV susceptibility.

In summary, we undertook a visualization-based approach using 3D collagen to better characterize the dynamics of DC-HIV capture, retention, and transmission of virus to susceptible T cells. We describe a mechanism by which surface-bound HIV particles on motile DCs function as adhesive receptors to contact and restrain migrating T cells to facilitate DC-to-T cell viral spread. Subsequent activation of signaling cascade facilitated by Env:CD4 binding further modulates T cell migration behaviors to enhance HIV susceptibility, providing additional insights into cellular mechanisms that contribute to the exponential viral replication observed in lymphoid organs during acute infection.

Limitations of the Study

The present study examined DC:T cell interaction dynamics and activation of signaling pathways in the presence of HIV particles within a 3D collagen model to more closely recapitulate cell-cell contacts in lymph nodes. These studies are yet to be verified *in vivo* using multiphoton intravital microscopy (MP-IVM) (Murooka et al., 2012; Murooka and Mempel, 2013; Usmani et al., 2019), where interactions with stromal and other immune lymph node cells in the presence of physiological blood and lymph flow can further modulate DC:T cell conjugate formations. The current study was also limited to monocyte-derived dendritic cells to model HIV-capture dynamics in collagen, and thus further validation using primary DC subsets isolated from mucosal tissues is warranted.

Lead Contact

Further information and requests for resources and reagents should be directed to the Lead Contact, Dr. Thomas Murooka.

Materials Availability

All materials developed and used in this study will be made available upon request.

Data and Code Availability

Data and code used in this study will be made available upon request.

METHODS

All methods can be found in the accompanying Transparent Methods supplemental file.

SUPPLEMENTAL INFORMATION

Supplemental Information can be found online at https://doi.org/10.1016/j.isci.2020.101427.

ACKNOWLEDGMENTS

This study was supported by Canadian Institutes of Health Research (CIHR) grants PJT-155951, HB2 164064, and XGG-142962 (to T.T.M.), Research Manitoba new investigator award (to T.T.M.), Manitoba Medical Service Foundation (MMSF) operating grant (to T.T.M.), and a Research Manitoba postdoctoral fellowship (to W.H.K.). J.K. is funded by a Tier 2 Canada Research Chair in the Molecular Pathogenesis of Emerging and Re-Emerging Viruses provided by the Canadian Institutes of Health Research (Grant no. 950-231498).

The NIH AIDS Research and Reference Reagent Program provided MAGI-CCR5 cells and Raltegravir.

AUTHOR CONTRIBUTIONS

Conceptualization and methodology, W.H.K. and T.T.M.; Investigation, W.H.K., P.L., O.A., U.M., and R.H.; Resources, J.K. and R.P.; Writing W.H.K. and T.T.M. Funding Acquisition, W.H.K., J.K., and T.T.M.

DECLARATION OF INTERESTS

The authors declare no competing interests.

Received: April 15, 2020
Revised: June 24, 2020
Accepted: July 30, 2020
Published: August 21, 2020

REFERENCES

Akiyama, H., Ramirez, N.G.P., Gudheti, M.V., and Gummuluru, S. (2015). CD169-mediated trafficking of HIV to plasma membrane invaginations in dendritic cells attenuates efficacy of anti-gp120 broadly neutralizing antibodies. PLOS Pathogens *11*, e1004751.

Andreotti, A.H., Schwartzberg, P.L., Joseph, R.E., and Berg, L.J. (2010). T-cell signaling regulated by the tec family kinase, Itk. Csh Perspect. Biol. *2*, a002287.

Asano, K., Nabeyama, A., Miyake, Y., Qiu, C.-H., Kurita, A., Tomura, M., Kanagawa, O., Fujii, S.-i., and Tanaka, M. (2011). CD169-Positive macrophages dominate antitumor immunity by crosspresenting dead cell-associated antigens. Immunity *34*, 85–95.

Baggaley, R.F., White, R.G., and Boily, M.-C. (2010). HIV transmission risk through anal intercourse: systematic review, meta-analysis and implications for HIV prevention. Int. J. Epidemiol. *39*, 1048–1063.

Barreiro, O., Zamai, M., Yanez-Mo, M., Tejera, E., Lopez-Romero, P., Monk, P.N., Gratton, E., Caiolfa, V.R., and Sanchez-Madrid, F. (2008). Endothelial adhesion receptors are recruited to adherent leukocytes by inclusion in preformed tetraspanin nanoplatforms. J. Cell Biol. *183*, 527–542.

Bertram, K.M., Botting, R.A., Baharlou, H., Rhodes, J.W., Rana, H., Graham, J.D., Patrick, E., Fletcher, J., Plasto, T.M., Truong, N.R., et al. (2019). Identification of HIV transmitting CD11c(+) human epidermal dendritic cells. Nat. Commun. *10*, 2759.

Bousso, P., and Robey, E. (2003). Dynamics of CD8(+) T cell priming by dendritic cells in intact lymph nodes. Nat. Immunol. *4*, 579–585.

Bromley, S.K., Burack, W.R., Johnson, K.G., Somersalo, K., Sims, T.N., Sumen, C., Davis, M.M., Shaw, A.S., Allen, P.M., and Dustin, M.L. (2001). The immunological synapse. Annu. Rev. Immunol. *19*, 375–396.

Bromley, S.K., Peterson, D.A., Gunn, M.D., and Dustin, M.L. (2000). Cutting edge: hierarchy of chemokine receptor and TCR signals regulating T cell migration and proliferation. J. Immunol. *165*, 15–19.

Bromley, S.K., Thomas, S.Y., and Luster, A.D. (2005). Chemokine receptor CCR7 guides T cell exit from peripheral tissues and entry into afferent lymphatics. Nat. Immunol. *6*, 895–901.

Brown, M.N., Fintushel, S.R., Lee, M.H., Jennrich, S., Geherin, S.A., Hay, J.B., Butcher, E.C., and Debes, G.F. (2010). Chemoattractant receptors and lymphocyte egress from extralymphoid tissue: changing requirements during the course of inflammation. J. Immunol. *185*, 4873–4882.

Cameron, P.U., Freudenthal, P.S., Barker, J.M., Gezelter, S., Inaba, K., and Steinman, R.M. (1992). Dendritic cells exposed to human immunodeficiency virus type-1 transmit a vigorous cytopathic infection to $CD4^+$ T cells. Science *257*, 383–387.

Cavrois, M., Neidleman, J., Kreisberg, J.F., and Greene, W.C. (2007). In vitro derived dendritic cells trans-infect CD4 T cells primarily with surface-bound HIV-1 virions. PLoS Pathog. *3*, e4.

Cicala, C., Arthos, J., Censoplano, N., Cruz, C., Chung, E., Martinelli, E., Lempicki, R.A., Natarajan, V., VanRyk, D., Daucher, M., et al. (2006). HIV-1 gp120 induces NFAT nuclear translocation in resting CD4+ T-cells. Virology *345*, 105–114.

Crocker, P.R., Paulson, J.C., and Varki, A. (2007). Siglecs and their roles in the immune system. Nat. Rev. Immunol. 255–266.

Cuevas, B.D., Abell, A.N., and Johnson, G.L. (2007). Role of mitogen-activated protein kinase kinase kinases in signal integration. Oncogene *26*, 3159–3171.

Cunningham, A.L., Donaghy, H., Harman, A.N., Kim, M., and Turville, S.G. (2010). Manipulation of dendritic cell function by viruses. Curr. Opin. Microbiol. *13*, 524–529.

Czeloth, N., Bernhardt, G., Hofmann, F., Genth, H., and Forster, R. (2005). Sphingosine-1-Phosphate mediates migration of mature dendritic cells. J. Immunol. *175*, 2960–2967.

Debes, G.F., Arnold, C.N., Young, A.J., Krautwald, S., Lipp, M., Hay, J.B., and Butcher, E.C. (2005). Chemokine receptor CCR7 required for T lymphocyte exit from peripheral tissues. Nat. Immunol. *6*, 889–894.

Deruaz, M., Murooka, T.T., Ji, S., Gavin, M.A., Vrbanac, V.D., Lieberman, J., Tager, A.M., Mempel, T.R., and Luster, A.D. (2017). Chemoattractant-mediated leukocyte trafficking enables HIV dissemination from the genital mucosa. JCI insight *2*, e88533.

Douek, D.C., Brenchley, J.M., Betts, M.R., Ambrozak, D.R., Hill, B.J., Okamoto, Y., Casazza, J.P., Kuruppu, J., Kunstman, K., Wolinsky, S., et al. (2002). HIV preferentially infects HIV-specific CD4+ T cells. Nature *417*, 95–98.

Duncan, C.J.A., Williams, J.P., Schiffner, T., Gartner, K., Ochsenbauer, C., Kappes, J., Russell, R.A., Frater, J., and Sattentau, Q.J. (2014). High-multiplicity HIV-1 infection and neutralizing antibody evasion mediated by the macrophage-T cell virological synapse. J. Virol. *88*, 2025–2034.

Edgar, L.J., Kawasaki, N., Nycholat, C.M., and Paulson, J.C. (2019). Targeted delivery of antigen to activated CD169+ macrophages induces bias for expansion of CD8+ T cells. Cell Chem. Biol. *26*, 131–136.e4.

Fackler, O.T., Murooka, T.T., Imle, A., and Mempel, T.R. (2014). Adding new dimensions: towards an integrative understanding of HIV-1 spread. Nat. Rev. Microbiol. *12*, 563–574.

Felts, R.L., Narayan, K., Estes, J.D., Shi, D., Trubey, C.M., Fu, J., Hartnell, L.M., Ruthel, G.T., Schneider, D.K., Nagashima, K., et al. (2010). 3D visualization of HIV transfer at the virological synapse between dendritic cells and T cells. Proc. Natl. Acad. Sci. U S A *107*, 13336–13341.

Forster, R., Schubel, A., Breitfeld, D., Kremmer, E., Renner-Muller, I., Wolf, E., and Lipp, M. (1999). CCR7 coordinates the primary immune response by establishing functional microenvironments in secondary lymphoid organs. Cell *99*, 23–33.

Francois, F., and Klotman, M.E. (2003). Phosphatidylinositol 3-kinase regulates human immunodeficiency virus type 1 replication following viral entry in primary CD4+ T lymphocytes and macrophages. J. Virol. *77*, 2539–2549.

Geijtenbeek, T.B., Kwon, D.S., Torensma, R., van Vliet, S.J., van Duijnhoven, G.C., Middel, J., Cornelissen, I.L., Nottet, H.S., KewalRamani, V.N., Littman, D.R., et al. (2000). DC-SIGN, a dendritic cell-specific HIV-1-binding protein that enhances trans-infection of T cells. Cell *100*, 587–597.

Girard, J.-P., and Springer, T.A. (1995). High endothelial venules (HEVs): specialized endothelium for lymphocyte migration. Immunol. Today *16*, 449–457.

Goldman, F., Jensen, W.A., Johnson, G.L., Heasley, L., and Cambier, J.C. (1994). gp120 ligation of CD4 induces p56lck activation and TCR desensitization independent of TCR tyrosine phosphorylation. J. Immunol. *153*, 2905–2917.

Gollmann, G., Neuwirt, H., Tripp, C.H., Mueller, H., Konwalinka, G., Heufler, C., Romani, N., and Tiefenthaler, M. (2008). Sphingosine-1-phosphate receptor type-1 agonism impairs blood dendritic cell chemotaxis and skin dendritic cell migration to lymph nodes under inflammatory conditions. Int. Immunol. *20*, 911–923.

Gousset, K., Ablan, S.D., Coren, L.V., Ono, A., Soheilian, F., Nagashima, K., Ott, D.E., and Freed, E.O. (2008). Real-time visualization of HIV-1 GAG trafficking in infected macrophages. PLoS Pathog. *4*, e1000015.

Grabowska, J., Lopez-Venegas, M.A., Affandi, A.J., and Den Haan, J.M.M. (2018). CD169+ macrophages capture and dendritic cells instruct: the interplay of the gatekeeper and the general of the immune system. Front. Immunol. *9*, 1–14.

Gummuluru, S., Pina Ramirez, N.G., and Akiyama, H. (2014). CD169-dependent cell-associated HIV-1 transmission: a driver of virus dissemination. J. Infect. Dis. *210* (*Suppl 3*), S641–S647.

Haase, A.T. (2010). Targeting early infection to prevent HIV-1 mucosal transmission. Nature *464*, 217–223.

Haase, A.T. (2011). Early events in sexual transmission of HIV and SIV and opportunities for interventions. Annu. Rev. Med. *62*, 127–139.

Hammonds, J.E., Beeman, N., Ding, L., Takushi, S., Francis, A.C., Wang, J.J., Melikyan, G.B., and Spearman, P. (2017). Siglec-1 initiates formation of the virus-containing compartment and enhances macrophage-to-T cell transmission of HIV-1. PLoS Pathog. *13*, 1–28.

Hatch, S.C., Sardo, L., Chen, J., Burdick, R., Gorelick, R., Fivash, M.J., Pathak, V.K., and Hu, W.-S. (2013). Gag-dependent enrichment of HIV-1 RNA near the uropod membrane of polarized T cells. J. Virol. *87*, 11912–11915.

Henrickson, S.E., Mempel, T.R., Mazo, I.B., Liu, B., Artyomov, M.N., Zheng, H., Peixoto, A., Flynn, M.P., Senman, B., Junt, T., et al. (2008). T cell sensing of antigen dose governs interactive behavior with dendritic cells and sets a threshold for T cell activation. Nat. Immunol. *9*, 282–291.

Hioe, C.E., Tuen, M., Vasiliver-Shamis, G., Alvarez, Y., Prins, K.C., Banerjee, S., Nádas, A., Cho, M.W., Dustin, M.L., and Kachlany, S.C. (2011). HIV envelope gp120 activates LFA-1 on CD4 T-lymphocytes and increases cell susceptibility to LFA-1-targeting leukotoxin (LtxA). PLoS One *6*, 1–11.

Hladik, F., Sakchalathorn, P., Ballweber, L., Lentz, G., Fialkow, M., Eschenbach, D., and McElrath, M.J. (2007). Initial events in establishing vaginal entry and infection by human immunodeficiency virus type-1. Immunity *26*, 257–270.

Hu, J., Gardner, M.B., and Miller, C.J. (2000). Simian immunodeficiency virus rapidly penetrates the cervicovaginal mucosa after intravaginal inoculation and infects intraepithelial dendritic cells. J. Virol. *74*, 6087–6095.

Hu, Q., Frank, I., Williams, V., Santos, J.J., Watts, P., Griffin, G.E., Moore, J.P., Pope, M., and Shattock, R.J. (2004). Blockade of attachment and fusion receptors inhibits HIV-1 infection of human cervical tissue. J. Exp. Med. *199*, 1065–1075.

Idzko, M., Panther, E., Corinti, S., Morelli, A., Ferrari, D., Herouy, Y., Dichmann, S., Mockenhaupt, M., Gebicke-Haerter, P., Di Virgilio, F., et al. (2002). Sphingosine 1-phosphate induces chemotaxis of immature and modulates cytokine-release in mature human dendritic cells for emergence of Th2 immune responses. FASEB J. *16*, 625–627.

Izquierdo-Useros, N., Blanco, J., Erkizia, I., Fernandez-Figueras, M.T., Borras, F.E., Naranjo-Gomez, M., Bofill, M., Ruiz, L., Clotet, B., and Martinez-Picado, J. (2007). Maturation of blood-derived dendritic cells enhances human immunodeficiency virus type 1 capture and transmission. J. Virol. *81*, 7559–7570.

Izquierdo-Useros, N., Lorizate, M., Contreras, F.X., Rodriguez-Plata, M.T., Glass, B., Erkizia, I., Prado, J.G., Casas, J., Fabriàs, G., Kräusslich, H.G., et al. (2012a). Sialyllactose in viral membrane gangliosides is a novel molecular recognition pattern for mature dendritic cell capture of HIV-1. PLoS Biol. *10*, e1001315.

Izquierdo-Useros, N., Lorizate, M., McLaren, P.J., Telenti, A., Krausslich, H.G., and Martinez-Picado, J. (2014). HIV-1 capture and transmission by dendritic cells: the role of viral glycolipids and the cellular receptor Siglec-1. PLoS Pathog. *10*, e1004146.

Izquierdo-Useros, N., Lorizate, M., Puertas, M.C., Rodriguez-Plata, M.T., Zangger, N., Erikson, E., Pino, M., Erkizia, I., Glass, B., Clotet, B., et al. (2012b). Siglec-1 is a novel dendritic cell receptor that mediates HIV-1 trans-infection through recognition of viral membrane gangliosides. PLoS Biol. *10*, e1001448.

Jacque, J.M., Mann, A., Enslen, H., Sharova, N., Brichacek, B., Davis, R.J., and Stevenson, M. (1998). Modulation of HIV-1 infectivity by MAPK, a virion-associated kinase. EMBO J. *17*, 2607–2618.

Jolly, C., Kashefi, K., Hollinshead, M., and Sattentau, Q.J. (2004). HIV-1 cell to cell transfer across an env-induced, actin-dependent synapse. J. Exp. Med. *199*, 283–293.

Jolly, C., Mitar, I., and Sattentau, Q.J. (2007). Adhesion molecule interactions facilitate human immunodeficiency virus type 1-induced virological synapse formation between T cells. J. Virol. 13916–13921.

Jolly, C., and Sattentau, Q.J. (2004). Retroviral spread by induction of virological synapses. Traffic *5*, 643–650.

Jolly, C., and Sattentau, Q.J. (2005). Human immunodeficiency virus type 1 virological synapse formation in T cells requires lipid raft integrity. J. Virol. *79*, 12088–12094.

Junt, T., Moseman, E.A., Iannacone, M., Massberg, S., Lang, P.A., Boes, M., Fink, K., Henrickson, S.E., Shayakhmetov, D.M., Di Paolo, N.C., et al. (2007). Subcapsular sinus macrophages in lymph nodes clear lymph-borne viruses and present them to antiviral B cells. Nature *450*, 110–114.

Juszczak, R.J., Turchin, H., Truneh, A., Culp, J., and Kassis, S. (1991). Effect of human immunodeficiency virus gp120 glycoprotein on the association of the protein tyrosine kinase p56lck with CD4 in human T lymphocytes. J. Biol. Chem. *266*, 11176–11183.

Klemke, R.L., Cai, S., Giannini, A.L., Gallagher, P.J., de Lanerolle, P., and Cheresh, D.A. (1997). Regulation of cell motility by mitogen-activated protein kinase. J. Cell Biol. *137*, 481–492.

Krueger, J.S., Keshamouni, V.G., Atanaskova, N., and Reddy, K.B. (2001). Temporal and quantitative regulation of mitogen-activated protein kinase (MAPK) modulates cell motility and invasion. Oncogene *20*, 4209–4218.

Laguette, N., Sobhian, B., Casartelli, N., Ringeard, M., Chable-Bessia, C., Segeral, E., Yatim, A., Emiliani, S., Schwartz, O., and Benkirane, M. (2011). SAMHD1 is the dendritic- and myeloid-cell-specific HIV-1 restriction factor counteracted by Vpx. Nature *474*, 654–657.

Lan, Y.Y., De Creus, A., Colvin, B.L., Abe, M., Brinkmann, V., Coates, P.T.H., and Thomson, A.W. (2005). The sphingosine-1-phosphate receptor agonist FTY720 modulates dendritic cell trafficking in vivo. Am. J. Transpl. *5*, 2649–2659.

Lan, Y.Y., Tokita, D., Wang, Z., Wang, H.C., Zhan, J., Brinkmann, V., and Thomson, A.W. (2008). Sphingosine 1-phosphate receptor agonism impairs skin dendritic cell migration and homing to secondary lymphoid tissue: association with prolonged allograft survival. Transpl. Immunol. *20*, 88–94.

Laufer, J.M., Kindinger, I., Artinger, M., Pauli, A., and Legler, D.F. (2018). CCR7 is recruited to the immunological synapse, acts as Co-stimulatory molecule and drives LFA-1 clustering for efficient T cell adhesion through ZAP70. Front. Immunol. *9*, 3115.

Len, A.C.L., Starling, S., Shivkumar, M., and Jolly, C. (2017). HIV-1 activates T cell signaling independently of antigen to drive viral spread. Cell Rep. 1062–1074.

Lindquist, R.L., Shakhar, G., Dudziak, D., Wardemann, H., Eisenreich, T., Dustin, M.L., and Nussenzweig, M.C. (2004). Visualizing dendritic cell networks in vivo. Nat. Immunol. *18*, 1243–1250.

Lopez, P., Koh, W.H., Hnatiuk, R., and Murooka, T.T. (2019). HIV infection stabilizes macrophage:T cell interactions to promote cell-cell HIV spread. J. Virol. *93*, e00805–19.

Lore, K., Smed-Sorensen, A., Vasudevan, J., Mascola, J.R., and Koup, R.A. (2005). Myeloid and plasmacytoid dendritic cells transfer HIV-1 preferentially to antigen-specific CD4+ T cells. J. Exp. Med. *201*, 2023–2033.

Martín-Fontecha, A., Lanzavecchia, A., and Sallusto, F. (2009). Dendritic cell migration to peripheral lymph nodes. Handb. Exp. Pharmacol. *188*, 31–50.

Masurier, C., Salomon, B., Guettari, N., Pioche, C., Lachapelle, F., Guigon, M., and Klatzmann, D. (1998). Dendritic cells route human immunodeficiency virus to lymph nodes after vaginal or intravenous administration to mice. J. Virol. *72*, 7822–7829.

McDonald, D., Wu, L., Bohks, S.M., KewalRamani, V.N., Unutmaz, D., and Hope, T.J. (2003). Recruitment of HIV and its receptors to dendritic cell-T cell junctions. Science *300*, 1295–1297.

Melar, M., Ott, D.E., and Hope, T.J. (2007). Physiological levels of virion-associated human immunodeficiency virus type 1 envelope induce coreceptor-dependent calcium flux. J. Virol. *81*, 1773–1785.

Mempel, T.R., Henrickson, S.E., and von Andrian, U.H. (2004). T-cell priming by dendritic cells in lymph nodes occurs in three distinct phases. Nature *427*, 154–159.

Menager, M.M., and Littman, D.R. (2016). Actin dynamics regulates dendritic cell-mediated transfer of HIV-1 to T cells. Cell, 695–709.

Miller, C.J., Li, Q., Abel, K., Kim, E.Y., Ma, Z.M., Wietgrefe, S., La Franco-Scheuch, L., Compton, L., Duan, L., Shore, M.D., et al. (2005). Propagation and dissemination of infection after vaginal transmission of simian immunodeficiency virus. J. Virol. *79*, 9217–9227.

Miller, M.J., Hejazi, A.S., Wei, S.H., Cahalan, M.D., and Parker, I. (2004). T cell repertoire scanning is promoted by dynamic dendritic cell behavior and random T cell motility in the lymph node. Proc. Natl. Acad. Sci. U S A *101*, 998–1003.

Miller, M.J., Wei, S.H., Cahalan, M.D., and Parker, I. (2003). Autonomous T cell trafficking examined in vivo with intravital two-photon microscopy. Proc. Natl. Acad. Sci. U S A *100*, 2604–2609.

Murooka, T.T., Deruaz, M., Marangoni, F., Vrbanac, V.D., Seung, E., von Andrian, U.H., Tager, A.M., Luster, A.D., and Mempel, T.R. (2012). HIV-infected T cells are migratory vehicles for viral dissemination. Nature, 283–287.

Murooka, T.T., and Mempel, T.R. (2012). Multiphoton intravital microscopy to study lymphocyte motility in lymph nodes. Methods Mol. Biol. 247–257.

Murooka, T.T., and Mempel, T.R. (2013). Intravital microscopy in BLT-humanized mice to study cellular dynamics in HIV infection. J. Infect. Dis. *208*, S137–S144.

Nabel, G., and Baltimore, D. (1987). An inducible transcription factor activates expression of human immunodeficiency virus in T cells. Nature *326*, 711–713.

Nasr, N., Lai, J., Botting, R.A., Mercier, S.K., Harman, A.N., Kim, M., Turville, S., Center, R.J., Domagala, T., Gorry, P.R., et al. (2014). Inhibition of two temporal phases of HIV-1 transfer from primary Langerhans cells to T cells: the role of langerin. J. Immunol. *193*, 2554–2564.

Nickol, M.E., Ciric, J., Falcinelli, S.D., Chertow, D.S., and Kindrachuk, J. (2019). Characterization of host and bacterial contributions to lung barrier dysfunction following Co-infection with 2009 pandemic influenza and methicillin resistant Staphylococcus aureus. Viruses *11*, 116.

Pena-Cruz, V., Agosto, L.M., Akiyama, H., Olson, A., Moreau, Y., Larrieux, J.R., Henderson, A., Gummuluru, S., and Sagar, M. (2018). HIV-1 replicates and persists in vaginal epithelial dendritic cells. J. Clin. Invest. *128*, 3439–3444.

Perez-Zsolt, D., Cantero-Pérez, J., Erkizia, I., Benet, S., Pino, M., Serra-Peinado, C., Hernández-Gallego, A., Castellví, J., Tapia, G., Arnau-Saz, V., et al. (2019). Dendritic cells from the cervical mucosa capture and transfer HIV-1 via Siglec-1. Front. Immunol. *10*, 1–14.

Permanyer, M., Bošnjak, B., and Förster, R. (2018). Dendritic cells, T cells and lymphatics: dialogues in migration and beyond. Curr. Opin. Immunol. *53*, 173–179.

Phan, T., Green, J., Gray, E., Xu, Y., and Cyster, J. (2009). Immune complex relay by subcapsular sinus macrophages and noncognate B cells drives antibody affinity maturation. Nat. Immunol. *10*, 786–793.

Piot, P., Abdool Karim, S.S., Hecht, R., Legido-Quigley, H., Buse, K., Stover, J., Resch, S., Ryckman, T., Mogedal, S., Dybul, M., et al. (2015). Defeating AIDS–advancing global health. Lancet *386*, 171–218.

Planas, D., Zhang, Y., Monteiro, P., Goulet, J.P., Gosselin, A., Grandvaux, N., Hope, T.J., Fassati, A., Routy, J.P., and Ancuta, P. (2017). HIV-1 selectively targets gut-homing CCR6+CD4+ T cells via mTOR-dependent mechanisms. JCI Insight *2*, e93230.

Platt, A.M., and Randolph, G.J. (2013). Dendritic cell migration through the lymphatic vasculature to lymph nodes. Adv. Immunol. *120*, 51–68.

Popik, W., Hesselgesser, J.E., and Pitha, P.M. (1998). Binding of human immunodeficiency virus type 1 to CD4 and CXCR4 receptors differentially regulates expression of inflammatory genes and activates the MEK/ERK signaling pathway. J. Virol. *72*, 6406–6413.

Randolph, G.J., Angeli, V., and Swartz, M.A. (2005). Dendritic-cell trafficking to lymph nodes through lymphatic vessels. Nat. Rev. Immunol. 617–628.

Rodriguez-Garcia, M., Shen, Z., Barr, F.D., Boesch, A.W., Ackerman, M.E., Kappes, J.C., Ochsenbauer, C., and Wira, C.R. (2017). Dendritic cells from the human female reproductive tract rapidly capture and respond to HIV. Mucosal Immunol. *10*, 531–544.

Rodriguez-Plata, M.T., Puigdomènech, I., Izquierdo-Useros, N., Puertas, M.C., Carrillo, J., Erkizia, I., Clotet, B., Blanco, J., and Martinez-Picado, J. (2013). The infectious synapse formed between mature dendritic cells and CD4(+) T cells is independent of the presence of the HIV-1 envelope glycoprotein. Retrovirology *10*, 42.

Rudnicka, D., and Schwartz, O. (2009). Intrusive HIV-1-infected cells. Nat. Immunol. *10*, 933–934.

Russo, E., Teijeira, A., Vaahtomeri, K., Willrodt, A.H., Bloch, J.S., Nitschke, M., Santambrogio, L., Kerjaschki, D., Sixt, M., and Halin, C. (2016). Intralymphatic CCL21 promotes tissue egress of dendritic cells through afferent lymphatic vessels. Cell Rep. *14*, 1723–1734.

Satpathy, A.T., Wu, X., Albring, J.C., and Murphy, K.M. (2012). Re(de)fining the dendritic cell lineage. Nat. Immunol. *13*, 1145–1154.

Saunderson, S.C., Dunn, A.C., Crocker, P.R., and McLellan, A.D. (2014). CD169 mediates the capture of exosomes in spleen and lymph node. Blood, 208–216.

Schwartzberg, P.L., Finkelstein, L.D., and Readinger, J.A. (2005). TEC-family kinases: regulators of T-helper-cell differentiation. Nat. Rev. Immunol. *5*, 284–295.

Sewald, X., Ladinsky, M.S., Uchil, P.D., Beloor, J., Pi, R., Herrmann, C., Motamedi, N., Murooka, T.T., Brehm, M.A., Greiner, D.L., et al. (2015). Retroviruses use CD169-mediated trans-infection of permissive lymphocytes to establish infection. Science *350*, 563–567.

Sigal, A., Kim, J.T., Balazs, A.B., Dekel, E., Mayo, A., Milo, R., and Baltimore, D. (2011). Cell-to-cell spread of HIV permits ongoing replication despite antiretroviral therapy. Nature *477*, 95–98.

Starling, S., and Jolly, C. (2016). LFA-1 engagement triggers T cell polarization at the HIV-1 virological synapse. J. Virol. *90*, 9841–9854.

Stieh, D.J., Matias, E., Xu, H., Fought, A.J., Blanchard, J.L., Marx, P.A., Veazey, R.S., and Hope, T.J. (2016). Th17 cells are preferentially infected very early after vaginal transmission of SIV in macaques. Cell Host Microbe *19*, 529–540.

Suárez, H., Rocha-Perugini, V., Álvarez, S.S., and Yáñez-Mó, M. (2018). Tetraspanins, another piece in the HIV-1 replication puzzle. Front. Immunol. *9*, 1–9.

Symeonides, M., Murooka, T.T., Bellfy, L.N., Roy, N.H., Mempel, T.R., and Thali, M. (2015). HIV-1-induced small T cell syncytia can transfer virus particles to target cells through transient contacts. Viruses *7*, 6590–6603.

Tal, O., Lim, H.Y., Gurevich, I., Milo, I., Shipony, Z., Ng, L.G., Angeli, V., and Shakhar, G. (2011). DC mobilization from the skin requires docking to immobilized CCL21 on lymphatic endothelium and intralymphatic crawling. J. Exp. Med. *208*, 2141–2153.

Tebit, D.M., Ndembi, N., Weinberg, A., and Quiñones-Mateu, M.E. (2012). Mucosal transmission of human immunodeficiency virus. Current HIV research *10*, 3–8.

Trifonova, R.T., Bollman, B., Barteneva, N.S., and Lieberman, J. (2018). Myeloid cells in intact human cervical explants capture HIV and can transmit it to CD4 T cells. Front. Immunol. *9*, 2719.

Turville, S.G., Santos, J.J., Frank, I., Cameron, P.U., Wilkinson, J., Miranda-Saksena, M., Dable, J., Stossel, H., Romani, N., Piatak, M., Jr., et al. (2004). Immunodeficiency virus uptake, turnover, and 2-phase transfer in human dendritic cells. Blood *103*, 2170–2179.

Uchil, P.D., Pi, R., Haugh, K.A., Ladinsky, M.S., Ventura, J.D., Barrett, B.S., Santiago, M.L., Bjorkman, P.J., Kassiotis, G., Sewald, X., et al. (2018). A protective role for the lectin CD169/

siglec-1 against a pathogenic murine retrovirus. Cell Host Microbe *25*, 87–100.e10.

Usmani, S.M., Murooka, T.T., Deruaz, M., Koh, W.H., Sharaf, R.R., Di Pilato, M., Power, K.A., Lopez, P., Hnatiuk, R., Vrbanac, V.D., et al. (2019). HIV-1 balances the fitness costs and benefits of disrupting the host cell actin cytoskeleton early after mucosal transmission. Cell Host Microbe *25*, 73–86.e75.

Vasiliver-Shamis, G., Cho, M.W., Hioe, C.E., and Dustin, M.L. (2009). Human immunodeficiency virus type 1 envelope gp120-induced partial T-cell receptor signaling creates an F-actin-depleted zone in the virological synapse. J. Virol. *83*, 11341–11355.

Vasiliver-Shamis, G., Dustin, M.L., and Hioe, C.E. (2010). HIV-1 virological synapse is not simply a copycat of the immunological synapse. Viruses *2*, 1239–1260.

Vasiliver-Shamis, G., Tuen, M., Wu, T.W., Starr, T., Cameron, T.O., Thomson, R., Kaur, G., Liu, J., Visciano, M.L., Li, H., et al. (2008). Human immunodeficiency virus type 1 envelope gp120 induces a stop signal and virological synapse formation in noninfected CD4+ T cells. J. Virol. *82*, 9445–9457.

Veninga, H., Borg, E.G., Vreeman, K., Taylor, P.R., Kalay, H., van Kooyk, Y., Kraal, G., Martinez-Pomares, L., and den Haan, J.M. (2015). Antigen targeting reveals splenic CD169+ macrophages as promoters of germinal center B-cell responses. Eur. J. Immunol. *45*, 747–757.

Wang, J.-H., Kwas, C., and Wu, L. (2009). Intercellular adhesion molecule 1 (ICAM-1), but not ICAM-2 and -3, is important for dendritic cell-mediated human immunodeficiency virus type 1 transmission. J. Virol. *83*, 4195–4204.

Weber, M., Hauschild, R., Schwarz, J., Moussion, C., de Vries, I., Legler, D.F., Luther, S.A., Bollenbach, T., and Sixt, M. (2013). Interstitial dendritic cell guidance by haptotactic chemokine gradients. Science *339*, 328–332.

Weissman, D., Rabin, R.L., Arthos, J., Rubbert, A., Dybul, M., Swofford, R., Venkatesan, S., Farber, J.M., and Fauci, A.S. (1997). Macrophage-tropic HIV and SIV envelope proteins induce a signal through the CCR5 chemokine receptor. Nature *389*, 981–985.

Whitney, J.B., Hill, A.L., Sanisetty, S., Penaloza-MacMaster, P., Liu, J., Shetty, M., Parenteau, L., Cabral, C., Shields, J., Blackmore, S., et al. (2014). Rapid seeding of the viral reservoir prior to SIV viraemia in rhesus monkeys. Nature *512*, 74–77.

Whitney, J.B., Lim, S.Y., Osuna, C.E., Kublin, J.L., Chen, E., Yoon, G., Liu, P.T., Abbink, P., Borducci, E.N., Hill, A., et al. (2018). Prevention of SIVmac251 reservoir seeding in rhesus monkeys by early antiretroviral therapy. Nat. Commun. *9*, 5429.

World Health Organization. (2018). Monitoring health for the SDGs, sustainable development goals. In Health Statistics 2018 (World Health Organization), pp. 4–12.

Wu, L., and KewalRamani, V.N. (2006). Dendritic-cell interactions with HIV: infection and viral dissemination. Nat. Rev. Immunol. *6*, 859–868.

Yang, X., and Gabuzda, D. (1999). Regulation of human immunodeficiency virus type 1 infectivity by the ERK mitogen-activated protein kinase signaling pathway. J. Virol. *73*, 3460–3466.

Yu, H.J., Reuter, M.A., and McDonald, D. (2008). HIV traffics through a specialized, surface-accessible intracellular compartment during trans-infection of T cells by mature dendritic cells. PLoS Pathog. *4*, e1000134.

Zhu, P., Liu, J., Bess, J., Jr., Chertova, E., Lifson, J.D., Grise, H., Ofek, G.A., Taylor, K.A., and Roux, K.H. (2006). Distribution and three-dimensional structure of AIDS virus envelope spikes. Nature *441*, 847–852.

iScience, Volume *23*

Supplemental Information

HIV-Captured DCs Regulate T Cell Migration and Cell-Cell Contact Dynamics to Enhance Viral Spread

Wan Hon Koh, Paul Lopez, Oluwaseun Ajibola, Roshan Parvarchian, Umar Mohammad, Ryan Hnatiuk, Jason Kindrachuk, and Thomas T. Murooka

KEY RESOURCES TABLE

REAGENT or RESOURCE	SOURCE	IDENTIFIER
Antibodies		
Human CD3	Biolegend	clone: HIT3a
Human CD4	Biolegend	clone: RPA-T4
Human CD11c	Biolegend	clone: Bu15
Human CD14	Biolegend	clone: 63D3
Human CD80	Biolegend	clone: 2D10
Human CD81	Biolegend	clone 5A6
Human CD83	Biolegend	clone: HB15E
Human CD86	Biolegend	clone: IT2.2
Human CD169	Biolegend	clone: 7-239
Human CD209	Biolegend	clone: 9E9A8
Human CCR7	Biolegend	clone: G043H7
Human CD11+CD18 (high affinity conformation)	Abcam	clone: 24
PSGL-1	Biolegend	clone KPL-1
goat anti-mouse IgG antibody conjugated with AF568	Thermo Scientific	Cat #A11004
Neutralizing Siglec-1 antibody	R&D	Cat #AF5197-SP
Human LFA-1	BD Biosciences	clone L130
Human ICAM-1	BD Biosciences	clone LB-2
Neutralizing CCR7 antibody	R&D	MAB197R-SP
Mouse LYVE-1	R&D	Clone: 223322
anti-human CD3ε/CD28 antibody coated dynabeads	Life Technologies	Cat #11131D
LPS from Salmonella Minnesota	Invivo Gen	Cat # tlrl-smlps
Fetal calf serum	VWR Seradigm	Cat #1500-500
Nunclon Sphera flasks	Thermo Scientific	Cat #174951
Bovine collagen	PureCol	Cat #5005-100ML
Dynasore hydrate	Sigma	Cat #D7693
Texas Red conjugated dextran (70kDa)	Thermo Scientific	Cat #D-1830
Texas Red conjugated phalloidin	Thermo Scientific	Cat #T7471
Collagenase D	Roche	Cat #11088866001
Bacterial and Virus Strains		
HIV-iGag/dTomato (BaL envelope)	This paper	N/A
HIV-iGag/dTomato Δenv (BaL envelope)	This paper	N/A
Biological Samples		
Chemicals, Peptides, and Recombinant Proteins		
human CCL19	Biolegend	Cat #582102

human CCL21	Biolegend	Cat #582202
human S1P	Sigma	Cat #73914
Human IL-4	Biolegend	Cat #574008
Human IL-2	Peprotech	Cat #200-02
Human GM-CSF	Biolegend	Cat #578606
FTY720-phosphate	Caymen	Cat #10008639
Raltegravir	NIH ARRRP	Cat# 11680
Critical Commercial Assays		
GenElute HP Plasmid Maxiprep Kit	Sigma	NA0310-1KT
Human CD14+ monocyte isolation kit	Stemcell Technologies	Cat #17858
Human CD4+ T cell isolation kit	Stemcell Technologies	Cat #17952
Deposited Data		
Experimental Models: Cell Lines		
HEK 293T cells	ATCC	ATCC CRL-11268
MAGI CCR5 cells	NIH ARRRP	Cat #3580
Experimental Models: Organisms/Strains		
Oligonucleotides		
Recombinant DNA		
Software and Algorithms		
Imaris 8.2	Bitplane	
ImageJ	NIH/freeware	
Prism 6	GraphPad	
FlowJo	Treestar	
Matlab	Mathworks	
Ingenuity pathway analysis (IPA)	Ingenuity Systems	
InnateDB	www.innatedb.com	
Other		

CONTACT FOR REAGENT AND RESOURCE SHARING

Further information and requests for resources and reagents should be directed to and will be fulfilled by the Lead Contact, Thomas Murooka (thomas.murooka@umanitoba.ca).

EXPERIMENTAL MODEL AND SUBJECT DETAILS

Cells

Human $CD14^+$ monocytes and $CD4^+$ T cells (both from Stem cell Technologies) were isolated from PBMCs of healthy donors (NetCAD, Canadian Blood Services). All cells derived from donors are anonymized and contain no information regarding the gender, race or health status. Studies using human blood products were approved by the University of Manitoba Biomedical Research Ethics Board (B2015:030).

MAGI.CCR5 cells were obtained from the NIH ARRRP (Cat #3522) and grown in DMEM supplemented with 10% fetal calf serum (VWR Seradigm), 2 mM GlutaMAX (Gibco), 1mM sodium pyruvate (Corning) and 10mM HEPES (Sigma-Aldrich) under 37°C/5% CO_2 conditions. The parental cell line of MAGI is a HeLa cell clone, which is a female cell line. This cell line has not been authenticated.

Viral Constructs and Preparation of Viral Stocks

The R5-tropic HIV Gag-iGFP/dTomato (HIV-iGFP for short) reporter encodes for two fluorescent proteins: (1) a fusion protein between GFP and the structural polypeptide Gag (Gag-iGFP) to visualize GFP-containing HIV particles (Muller et al., 2004), and (2) a *nef-IRES-dTomato* gene cassette that express soluble dTomato (Usmani et al., 2019) after productive infection. The *env*-deleted plasmid was constructed by digesting the HIV Gag-iGFP plasmid

with PsiI to generate a frameshift mutation in the *env* gene (HIV-iGFPΔ*env)*, as described previously (Murooka et al., 2012). All plasmids were confirmed by Sanger sequencing.
All HIV-1 stocks were generated by transient transfection of HEK 293T cells using calcium phosphate. To generate HIV-iGag virus, cells were co-transfected with the pGagPol plasmid (NIH ARRRP). Viral supernatants were collected 48 hours after transfection and layered over a 20% sucrose solution before ultra-centrifugation at 35,000 rpm for 90 min using an SW70Ti rotor (Beckman Coulter). Virus pellets were resuspended in PBS, aliquoted and stored at -80ºC until use. Each HIV stock was titrated using MAGI.CCR5 cells and expressed as infectious blue focus units (bfu) per ml.

METHOD DETAILS

Cell culture

Human $CD14^+$ monocytes and $CD4^+$ T cells (Stem cell Technologies) were isolated from PBMCs of healthy donors (NetCAD, Canadian Blood Services). Cell purity for both populations were routinely >95%. Monocytes were differentiated into immature dendritic cells by seeding into Nunclon™ Sphera™ flasks (Thermo Scientific) with 50ng/mL each of human granulocyte-macrophage colony-stimulating factor (hGM-CSF; Biolegend) and interleukin 4 (IL-4; Biolegend) in complete RPMI1640 media supplemented with 10% FBS (VWR Seradigm), 2 mM GlutaMAX (Gibco), 1mM sodium pyruvate (Corning Cat #25-000-CI) and 10mM HEPES (Sigma-Aldrich), for five days. On day 5, immature monocyte-derived dendritic cells (MDDCs) were stimulated with 100ng/mL purified lipopolysaccharide (LPS) from *Salmonella minnesota* (Invivo Gen) for 24-48 hours. Naïve CD4+ T cells were activated with anti-human CD3ε/CD28 antibody coated dynabeads (1:1 bead:cell ratio, Life Technologies) in complete RPMI 1640

media. After two days, beads were magnetically removed and T cells were cultured for another 4-6 days in complete medium containing 50 IU/mL human rIL-2 (Peprotech), keeping cell densities at 2 x 10^5 cells/mL. Day 7 expanded T cells were used for all experiments. Studies using human blood products were approved by the University of Manitoba Biomedical Research Ethics Board (B2015:030).

Flow cytometry and antibodies

Phenotypic characterization of MDDCs and CD4+ T cells were performed using the BD FACSCanto-II and analyzed with FlowJo software (Tree Star). Human Fc receptors (FcR) blockade was performed using the TruStain FcX™ (Biolegend) solution. MDDC and T cells were phenotyped with a panel of directly conjugated anti-human mAb (Biolegends) as indicated in the Key Resources Table. HIV-captured DCs and HIV infected T cells were fixed with 2.5% paraformaldehyde prior to flow cytometry analysis.

Virus capture and retention assays

3-6 million DCs were pulsed with HIV-iGFP (1,550 – 3,300 bfu) and their capture efficiency measured by flow cytometry. Because HIV-iGFPΔ*env* titers were not attainable using MAGI.CCR5 indicator cell lines, we pulsed DCs with increasing amounts of either parental or HIV-iGFPΔ*env* stocks to achieve equivalent numbers of HIV-captured DCs by flow cytometry (data not shown). To evaluate the role of Siglec-1 on HIV capture efficiency, DCs were pre-treated with anti-Siglec-1 neutralizing antibody (2ug; R&D) for 15 mins at room temperature prior to virus incubation and imaging studies.

Live-cell imaging in 3D collagen chambers

Collagen type I was used to recapitulate the three-dimensional (3D) fibrillar networks found in the lymph node T cell zone (Wolf et al., 2009) and were assembled as previously described (Sixt and Lammermann, 2011). Bovine collagen (PureCol) was used to achieve a final concentration of 1.7mg/mL in each chamber. To characterize the HIV capture dynamics by DCs, 1-2 million DCs were labeled with Celltracker Blue (CMAC; 30μM) or Celltracker Red (CMTPX; 7.5μM), washed and embedded into collagen along with HIV particles. Chambers were allowed to solidify for 45 minutes at 37°C / 5% CO_2 and placed onto a custom-made heating platform attached to a temperature controller apparatus (Werner Instruments). A thermocouple device was used to continuously monitor and maintain the chamber temperature at 37°C. A multiphoton microscope with two Ti:sapphire lasers (Coherent) was tuned to between 780 and 920 nm for optimized excitation of the fluorescent probes used. For four-dimensional recordings of cell migration, stacks of 13 (or 26) optical sections (512 x 512 pixels) with 4 μm z-spacing were acquired every 15 (or 30) seconds to provide imaging volumes of 48 (or 96) μm in depth. Emitted light was detected through 460/50 nm, 525/70 nm and 595/50 nm dichroic filters with non-descanned detectors. All images were acquired using the 20X 1.0 N.A. Olympus objective lens (XLUMPLFLN; 2.0mm WD).

To perform live imaging studies of antibody-labeled DCs, DCs were pulsed with HIV particles for 4 hours, washed extensively with warm complete media to remove free virus, and then incubated with primary antibodies against Siglec-1, PSGL-1 and CD81. Secondary goat anti-mouse IgG antibody conjugated with Alexa Fluor 568 or Alexa Fluor 594 (Thermo Fisher Scientific) were added at 1:100 dilution for an additional 15 minutes, then cells were washed and embedded into collagen chambers for imaging studies. In some experiments, cells were

pretreated with either isotype or blocking antibodies for LFA-1 (BD Biosciences), CD4 (Biolegend) or ICAM-1 (BD Biosciences) prior to embedding into collagen chambers. To study the role of actin, CMAC-labeled cells were pre-treated with Dynasore (100μM) for 20 mins at room temperature and embedded into collagen chambers with HIV particles. As Dynasore is a reversible drug, for some experiments, Dynasore were washed out after 2 hours of incubation. These washed cells were then embedded with HIV-1 particles in the collagen chamber. In some studies, HIV-captured DCs were pulsed with Texas Red-conjugated dextran (70kDa; Thermo Fisher Scientific) for 15 mins at 37°C prior to embedding into collagen chambers. A 1:4 or 1:8 ratio of DCs and CD4 T cells, respectively, was used for visualizing cell-cell contact dynamics in collagen chambers.

Immunofluorescent staining in collagen chambers

To preserve the migratory DC morphology in collagen, chambers were fixed with 4% paraformaldehyde/5% sucrose overnight at 37°C / 5% CO_2, as described previously (Lopez et al., 2019). Glycine buffer (0.15M) was used to quench residual PFA. Next, chambers were permeabilized using a 0.5% triton-X solution for 48 hours at 4°C. Collagen gels were blocked using 1% bovine albumin serum (BSA) and labeled with Texas Red™-conjugated phalloidin (ThermoFisher), as per manufacturer's protocol.

Transmission electron microscopy

Transmission electron microscopy was performed to reveal the ultrastructure of the HIV-containing compartments in migratory DCs in collagen. DC-embedded chambers were fixed, quenched with glycine buffer and incubated in 0.05% Tween in PBS. Gels were fixed with 1%

osmium tetroxide for 2 hours, then dehydrated using the following solutions: 30% ethanol, 50% ethanol, 70% ethanol, 90% ethanol, 100% ethanol, 100% methanol, then 100% propylene oxide. Gels were placed in embedding solution (mixture of EMbed 812, DDSA, NMA and DMP-30) for 24 hours prior to ultra-sectioning with the Reichert ultrathin microtome at a thickness of 70-90nm. The EM grids were then stained with uranyl acetate for 30 minutes and lead citrate for 10 minutes**.** Electron micrographs were taken with a Philips CM10 transmission electron microscope.

Transwell® assay

To investigate the chemotactic migration of HIV-bearing MDDCs towards lymph node chemokines, 0.5-1 million DCs were placed into the top insert at a final volume of 100µl of a Transwell plate (5µm pore size; Corning). 600µl of media containing human CCL19 (2ug; Biolegend) and CCL21 (2µg; Biolegend) or S_1P (10nM) was added to the bottom chamber. Transwell plates were incubated for 3 hours at 37°C/5% CO_2, after which migrated DCs in the bottom well were collected and counted using counting beads by flow cytometry (Biolegend). For receptor blockade studies, DCs were pre-treated with anti-CCR7 antibody (2µg; R&D) or FTY720-P (10 µM) prior to analysis in transwell assays.

***Ex vivo* skin crawl-in assay**

A crawl-in assay using explanted mouse ears was used to assess chemokine-dependent DC migration in the dermal layer in real time, as previously described, with some modifications (Weber and Sixt, 2013). Briefly, the ears of female/male 6-8-week-old Balb/c mice were excised, and ear sheets composed of the epidermis and dermis was obtained using forceps. After FcR

blockade, the lymphatic vessels were labeled with Alexa Fluor-594 conjugated mouse anti-LYVE-1 antibody (R&D) for 30 minutes at room temperature. Ear sheets were overlaid with 0.25 million DCs with or without HIV for 20 minutes at 37°C to allow them to crawl into the dermal layer. After washing away unbound DCs, skin sheets were mounted onto a glass slide with complete media and prepared for live-cell microscopy. In some studies, DCs were pre-treated with anti-CCR7 and/or FTY720 prior to overlay onto dermal tissue layers.

Image analysis

Time lapse micrograph images were transformed using Imaris 8.3 (Bitplane) to generate maximum intensity projections (MIPs) and exported as Quicktime movies. Automated 3D tracking of DC centroids was performed for all motility analyses, and subsequent cell track parameters (arrest coefficient, mean displacement) were analyzed using a custom script in Matlab (Mathworks). To characterize the spatial distribution of HIV-containing compartments in motile DCs, line profile analyses were performed to determine fluorescent intensity profiles on the z-axis, where 0 represents the uropodia and 1 represents the leading edge. Cell surface area and cell perimeter measurements were performed using ImageJ using the wand (tracing) tool after color thresholding. Circularity measurements were also performed using ImageJ, where a measure of 0 indicated a straight line and 1 indicated a perfect circle, as previously described (Usmani et al., 2019). Contact duration and cell migration speeds during contacts were analyzed using ImageJ.

HIV infection in collagen matrix

0.5 million DCs and 2-4 million CD4+ T cells were embedded into collagen gel with HIV particles and placed into a 48-well plate. Solidified gels were incubated for 4 hours at 37°C, then cells were recovered after digestion with collagenase D (Roche), washed and subsequently placed in complete media containing 50IU/mL hrIL-2 in a 24 well plate. T cells in the culture supernatant were gently removed, whereas DCs remained attached to the plastic culture vessel (which removed >95% of DCs). Recovered T cells were incubated for another 48 hours and productive infection was assessed by flow cytometry. Cell-free infection in collagen matrix was performed in parallel but in the absence of DCs. In some experiments, cells were pretreated with either isotype or neutralizing antibodies prior and during DC co-cultures in collagen. Raltegravir (20μM) was used to prevent productive infection and served as a negative control.

Phenotypic analysis of high affinity LFA-1

One million DCs were pulsed with HIV (WT and Δ*env*) for 3 hours and washed with RPMI medium to remove unbound virus. DCs were co-cultured with 4 million resting autologous CD4+ T cells in collagen gel for 3.5 hours. T cells were recovered using collagenase D and were immediately stained for high affinity LFA-1 expression (Human CD11+CD18, clone 24) for flow cytometry analysis.

Kinome analysis

Design, construction and application of the human peptide arrays were based on a previously reported protocol (Kindrachuk et al., 2014). DCs were pulsed with either wildtype or HIV-iGFP*ΔEnv*, washed extensively and co-cultured with autologous T cells for 15 minutes at 37°C. Cells were placed on ice and T cells were separated using a negative selection magnetic column

to remove $CD11c^+$ DCs (purity >98%). T cells were pelleted, cell lysates prepared and incubated with human kinome arrays (JPT Technologies). Briefly, cell pellets were lysed with 100uL buffer (20 mM Tris-HCl, pH 7.5, 150 mM NaCl, 1 mM EDTA, 1 mM ethylene glycol tetraacetic acid, 1% Triton X-100, 2.5 mM sodium pyrophosphate, 1 mM Na_3VO_4, 1 mM NaF, 1 g/ml leupeptin, 1 g/ml aprotinin, 1 mM phenylmethylsulfonyl fluoride) and incubated on ice for 10 min. Cell lysates were clarified by centrifugation at 14,000 rpm. Cell lysates were transferred to fresh microcentrifuge tubes, and the total protein concentrations were measured using the Pierce BCA Protein Assay Kit. Activation mix (50% glycerol, 50 μM ATP, 60 mM MgCl2, 0.05% Brij 35, 0.25 mg/mL bovine serum albumin) was added to the equivalent amounts of total protein (100 μg) for each sample, and total sample volumes were matched by the addition of kinome lysis buffer. Samples were spotted onto kinome peptide arrays (JPT Peptide Technologies GmbH, Berlin, Germany) and incubated for 2 h at 37 °C and 5% CO2. Following incubation, arrays were washed once with PBS containing 1% Triton X-100, followed by a single wash in deionized H2O. Arrays were stained with PRO-Q Diamond phosphoprotein stain (Invitrogen, Carlsbad, CA, USA) for 1 h with gentle agitation. Arrays were subsequently destained (20% acetonitrile, 50 mM sodium acetate, pH 4.0) 3 times × 10 min each with the addition of fresh destain each time. A final 10 min wash was performed with deionized H2O. Arrays were dried by gentle centrifugation. Array images were acquired using a PowerScanner microarray scanner (Tecan, Morrisville, NC, USA) with a 580-nm filter to detect dye fluorescence. Signal intensity values were collected using Array-Pro Analyzer version 6.3 software (Media Cybernetics, Rockville, MD, USA).

Kinome data analysis

The specific responses of each peptide were calculated by subtracting background intensity from foreground intensity. Signal intensities induced by *ΔEnv* HIV-iGFP were subtracted from the intensities from the time-matched, wildtype HIV-iGFP biological conditions, and test statistics were calculated. Average intensities were then taken over the three replicate intensities, and these values were subjected to hierarchical clustering analysis using InnateDb (www.innatedb.com) and ingenuity pathway analysis (IPA) software (Ingenuity Systems, Redwood City, CA). For our investigations, input data were limited to peptides that showed consistent responses across the biological replicates ($p<0.05$) as well as statistically significant changes between the wildtype and ΔEnv HIV conditions to identify biological pathways that are specifically induced through Env:CD4 interactions. In Figure 6E, we used the IPA regulation z-score algorithm to identify biological functions that were above a z-score >1 (black bars), and p-values (red line), calculated with the Fischer's exact test, reflects the likelihood that the association between a set of active kinases and a biological function is significant [p-value < 0.05].

MATERIAL AVAILABILITY

HIV reporter plasmids generated in this study will be available to researchers upon request.

QUANTIFICATION AND STATISTICAL ANALYSIS

Unpaired Student's t test and Mann-Whitney U test were used for comparisons of datasets with normal and non-normal distribution, respectively, using Prism 5 (GraphPad). Median and p

values from statistical analyses are indicated in each graph. When p values were higher than 0.05, differences were considered as not significant.

DATA AND SOFTWARE AVAILABILITY

MATLAB cell motility analysis scripts will be made available upon request. Motility parameters were calculated as described by Beltman et al. (2009). Briefly, mean velocities were defined as the average of the distance a cell traveled over the time period between the two consecutive frames. Confinement ratio is calculated based as the ratio of the displacement a cell has traveled over the total length of the path that cell has travelled. Figures and illustrations were prepared using Adobe® Illustrator and BioRender.com.

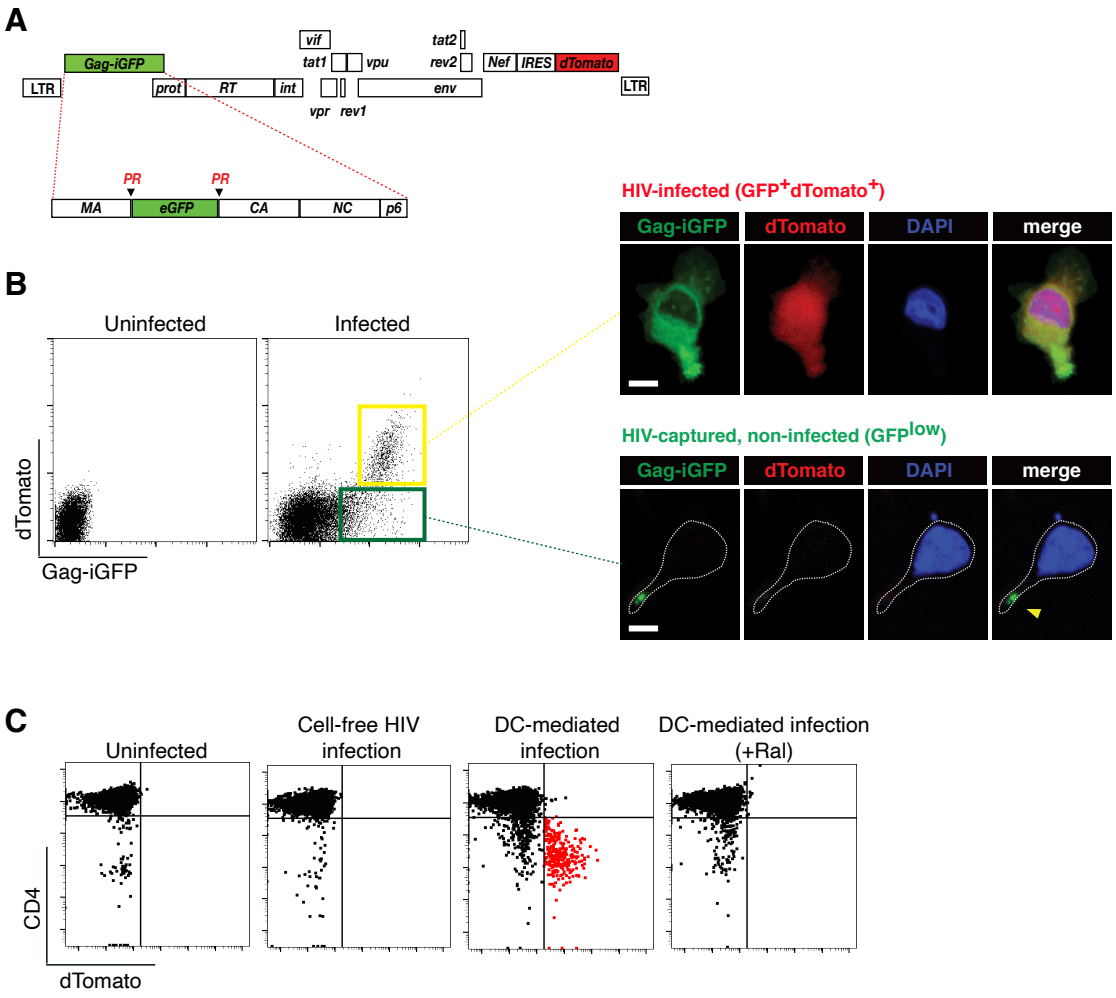

Supplementary Figure 1: Schematic and validation of the HIV Gag-iGFP/dTomato reporter, Related to Figure 1 and 4. (A) Schematic illustration of the reporter proviral vector. PR = protease cleavage sites. **(B)** T cells were infected with HIV-iGFP and characterized by flow cytometry and confocal microscopy. **(C)** T cells were infected with HIV-iGFP in the presence or absence of DCs, and assessed for infection after 48 hours. Raltegravir was added at the time of infection to serve as control. The presence of DCs enhanced T cell infection, and productively infected dTomato+ T cells (red dots) downregulate CD4 expression, as expected. Representative data from 3 independent experiments are shown.

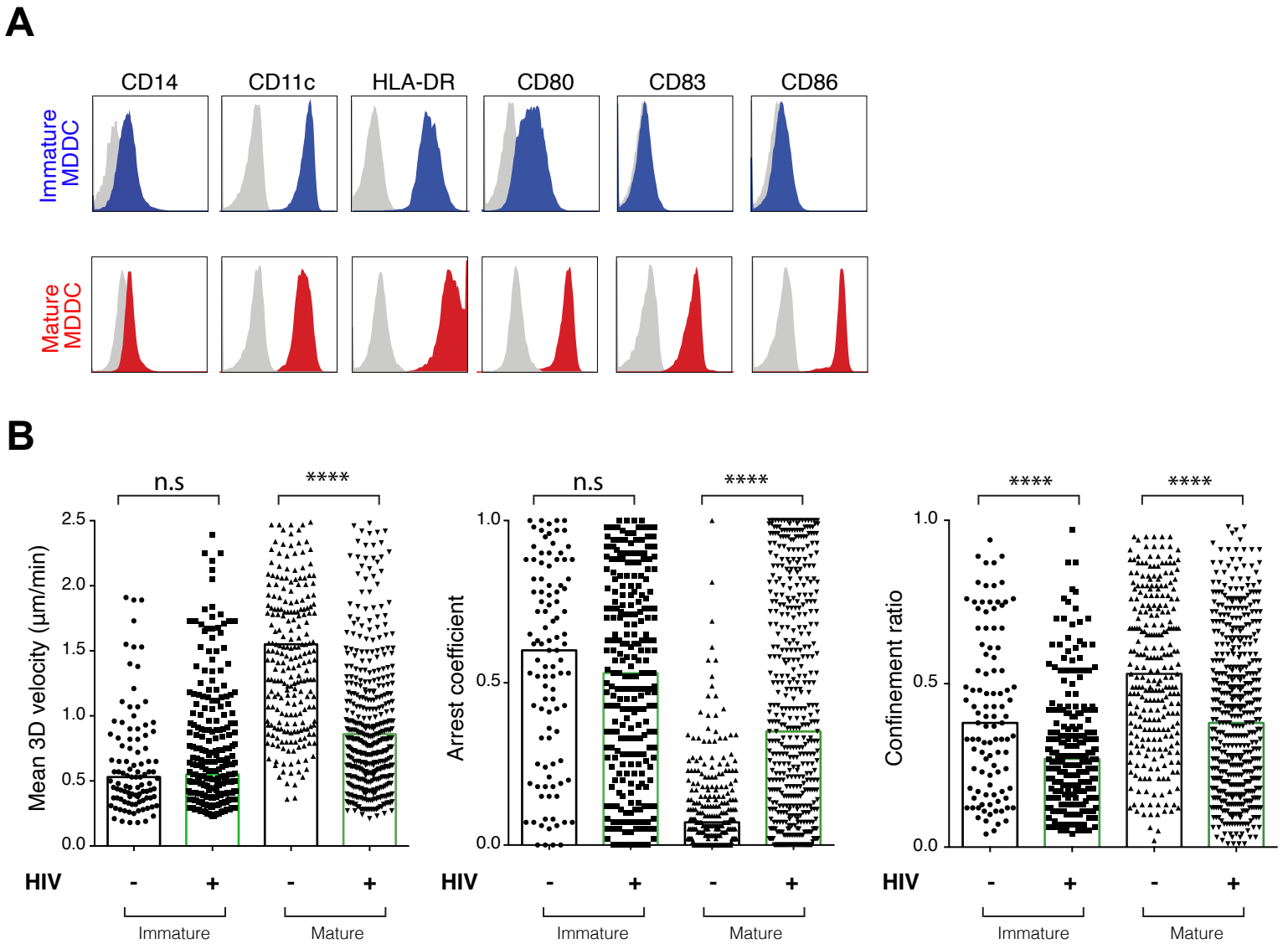

Supplementary Figure 2: 3D migration behavior of mature DCs after HIV exposure, Related to Figure 1.
(A) Phenotypic analysis of monocyte-derived dendritic cells (MDDCs) before and after stimulation with LPS for 24 hours. **(B)** Immature or mature DCs were either left alone or exposed to HIV-iGFP for 4 hours, washed, and embedded into collagen chamber for live-cell microscopy studies. Each data point represents a single cell. Bar graph indicate median values. Cumulative data from 3 independent experiments are shown. n.s. = not significant. **** $p \leq 0.001$

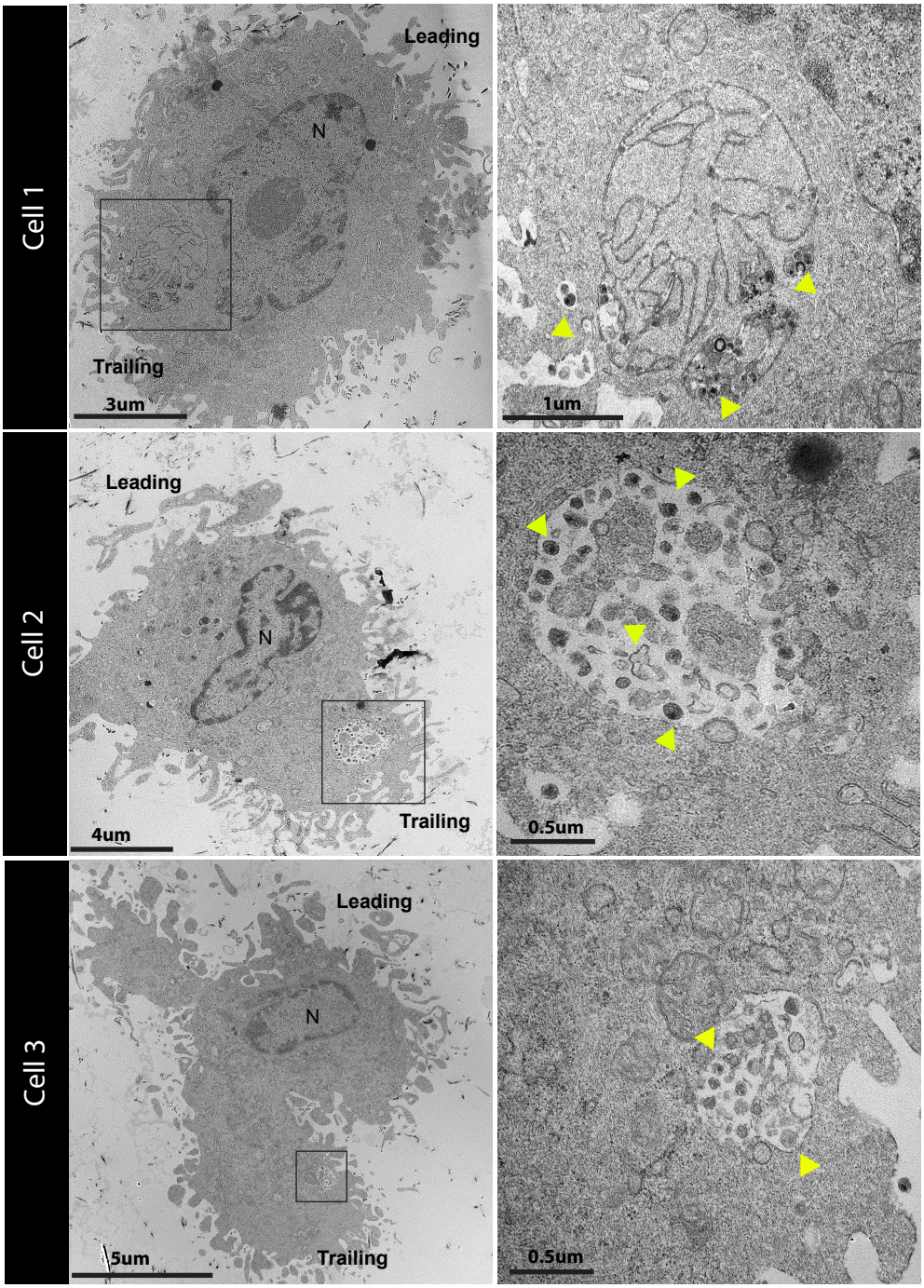

Supplementary Figure 3: Transmission electron micrograph of polarized HIV-captured DCs in collagen matrix, Related to Figure 2. Mature HIV particles are found in membrane invaginations close to the cell surface (yellow arrowheads in enlarged insets). The leading and trailiing edge are indicated, based on the location of the nucleus (N).

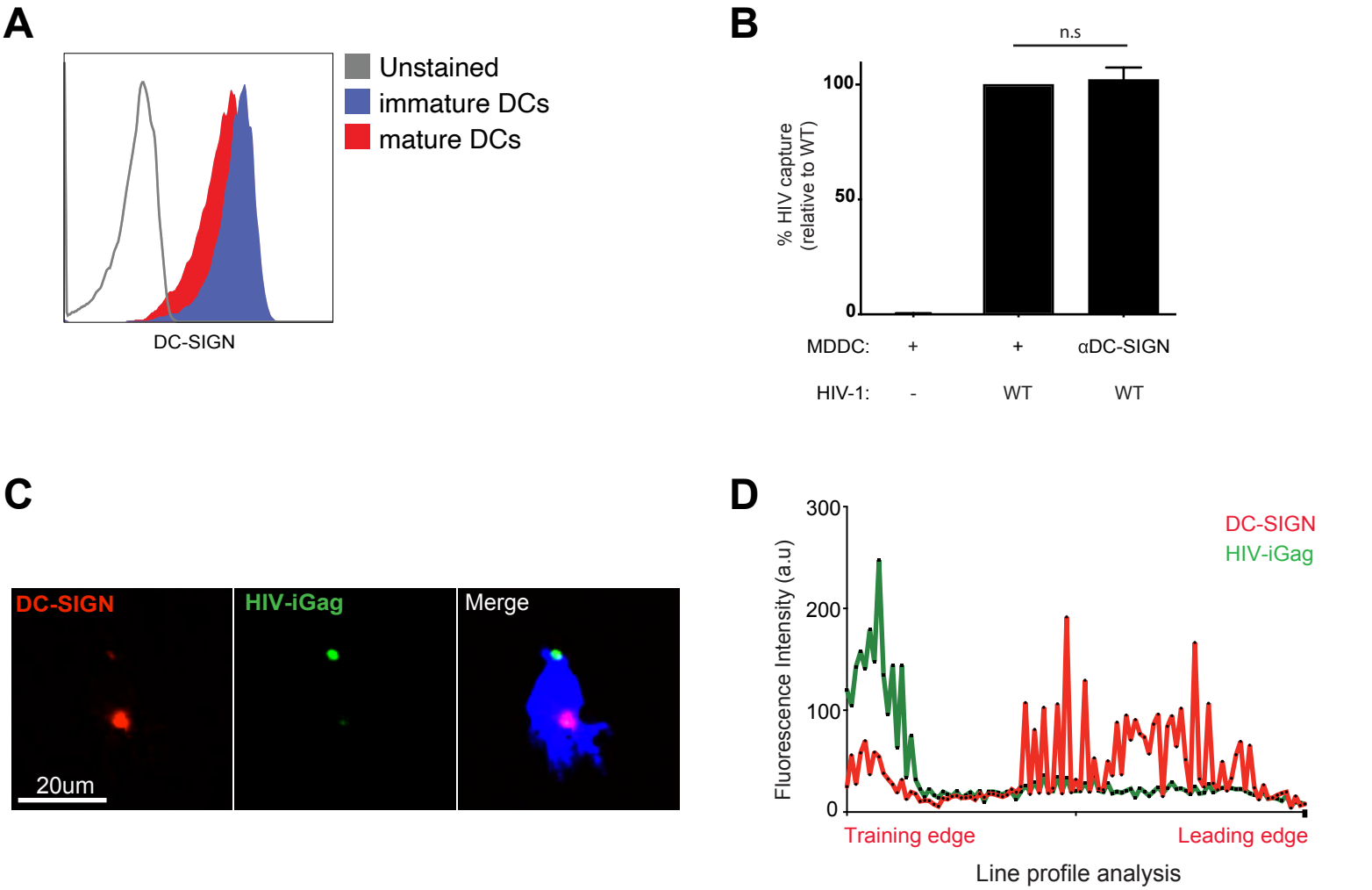

Supplementary Figure 4: DC-SIGN does not facilitate HIV capture by motile DCs in 3D collagen, Related to Figure 3. (A) Phenotypic expression of DC-SIGN between immature and mature MDDCs. (B)% HIV capture by DCs, relative to DCs treated with vehicle prior to incubation with virus. Representative data from two independent expeirments is shown. Mean +/- SEM. n.s. = not significant. (C) Representative micrograph of a HIV-captured DC in collagen matrix stained for DC-SIGN. (D) Representative line profile analysis of HIV-Gag-iGFP and DC-SIGN fluorescence intensity in a polarized HIV-captured DC shown in (B) (n=13).